A Study in Blue: Secondary Copper-rich Minerals and Their Associated Bacterial Diversity in Icelandic Lava Tubes

Nina Kopacz[1], Joleen Csuka[2], Mickael Baqué[3], Iaroslav Iakubivskyi[4], Hrefna Gulaugardóttir[5], Ingeborg J. Klarenberg[6], Mahid Ahmed[1], Alexandra Zetterlind[1], Abhijeet Singh[7], Inge Loes ten Kate[1], Eric Hellebrand[1], Brent R. Stockwell[2], Árni B. Stefánsson[8], Oddur Vilhelmsson[9], Anna Neubeck[7], Anna Schnürer[10], and Wolf Geppert[11]

[1]Utrecht University
[2]Columbia University
[3]German Aerospace Centre (DLR)
[4]University of Tartu
[5]University of Akureyri
[6]University of Akureyri, University of Iceland Biomedical Center
[7]Uppsala University
[8]Augnlæknastofa ÁBS
[9]University of Akureyri, University of Iceland Biomedical Center, University of Reading School of Biological Sciences
[10]Swedish University of Agricultural Sciences
[11]Stockholm University Astrobiology Center

November 24, 2022

Abstract

Lava tubes on Mars hold exciting potential for the preservation of biosignatures, which may survive on geological timescales in these isolated, stable environments. To support the development of future astrobiological mission concepts, we turn to terrestrial lava tubes, host to a variety of microbial communities and secondary minerals. Following a multidisciplinary sampling protocol, we retrieved biological, molecular, and mineralogical data from several lava tubes in Iceland. We report on blue-colored copper-rich secondary minerals and their associated bacterial communities using a multi-method approach, and an amalgam of 16S rRNA gene sequencing, Raman spectroscopy, scanning electron microscopy, and energy-dispersive X-ray spectroscopy data sets. We found numerous bacterial genera known for their high metal resistance and ability to survive in low-nutrient environments, both characteristics to be expected for any potential life in Martian lava tubes. Associated with them, we identified several types of copper-rich secondary minerals as well as carotenoid signals. If found in Martian lava tubes, blue copper-rich mineral precipitates would be deserving of astrobiological investigation, as they have potential to preserve biosignatures and harbor life.

1 Introduction

Cave environments on Earth have long provided shelter to a variety of organisms, from microbes to humans. Though their scales of interest differ vastly, these two examples have sought the same comfort from caves: a stable and sheltered environment, protected from the woes of the surface world. Since the discovery of lava caves on Mars (see (Sauro et al., 2020) for a review), they have become of renewed interest as targets for human shelter in future missions, as well as areas of astrobiological interest, with the potential of harboring traces of extant or extinct extraterrestrial life.

Recent years have seen a huge advancement in the development and miniaturization of autonomous mobility systems and exploration technologies for robotic missions to planetary caves, including instrument suites for *in situ* astrobiological studies (summarized in (Blank et al., 2020)). All aspects of cave mission preparation, from robotics development to astronaut training and scientific advancement, are currently being tested in terrestrial analogue sites, namely lava tubes in the Azores, Hawai'i, Iceland, Lanzarote, the western continental United States, and other volcanic areas.

Astrobiological studies in terrestrial lava tubes focus on the characterization of the microbe-mineral continuum and the identification of biosignatures in the form of biologically mediated speleothems (secondary cave minerals) and other geochemical fingerprints that may remain preserved on geological timescales (Boston et al., 2001; Léveillé & Datta, 2010; Northup et al., 2011; Northup & Lavoie, 2001). A suite of analyses is required to distinguish a biologically mediated secondary mineral from one that is abiotic (Uckert et al., 2017), presenting a difficult challenge**.** Nonetheless, a variety of biologically mediated speleothems has been reported in the literature, including filamentous manganese "snow", "crisco" moonmilk, lithified U-loops and living sulfuric acid "snotties", and pool fingers in limestone caves in New Mexico and Mexico (Boston et al., 2001).

Microbes in caves on Earth attach to minerals on cave walls, ceilings, or floors and initiate biomineralization reactions, creating biofilms. Biofilm formation is controlled by several processes, starting by initial microbe adhesion to the surface, governed by fluid flow and charging of the substratum. The initial colonizers excrete exopolysaccharides, which increase the surface irregularity and allow the biofilm to grow. Thus, the location of biofilm growth in caves depends not only on where particles and microbes can be transported to, but also be allowed to accumulate. A detailed review of the dynamics of biofilm formation on mineral surfaces and their spatial distribution is given by Little & Wagner (2018).

As the biofilm grows in layers away from the surface, it becomes a microbial mat of great complexity. Within its structure, chemical environments can exist that are radically different from that of the surrounding, allowing for the growth of minerals and microbes that would otherwise not be expected. Concentration of organic and inorganic particles can sustain a consortium of microorganisms of different nutritional modes. The putatively high microbial diversity within the biofilm may create local changes in pH or redox conditions, which can facilitate the precipitation of minerals that are unstable outside of the biofilm. Microbes can control the precipitation of these minerals either passively, where microbial cells act as nucleation sites, or actively, where bacterially produced enzymes control mineralization (Northup & Lavoie, 2001).

The majority of life in the Universe is thought to be unicellular (Schulze-Makuch & Irwin, 2018). Moreover, the tendency to form biofilms and mats may well be an adaptation to be expected on other planets, with other biologies, and perhaps other fundamental chemistries (Boston et al., 2001). Regardless of their specific chemistries, metabolisms relying on differences in redox potentials in elements present in the lava rock can be expected for any initial colonizers in Martian lava caves, due to the absence of light and the oligotrophic (low nutrient) quality of caves on Mars. The chemolithoautotrophic nature of this hypothetical life may eventuate the production of similar speleothems as found in terrestrial caves. Basaltic terrestrial lava tubes are most similar in mineralogy to those posited on Mars and may thus provide analogous potential for chemolithoautotrophy, resulting in similar, recognizable molecular markers and biologically mediated speleothems.

To prepare a multidisciplinary sampling protocol for future astrobiological missions to caves on Mars, we set up the Planetary Analogues and Exobiology Lava Tube Expedition (PELE). Since 2017, we have explored lava fields and lava tubes on Hawai'i, the Azores, and Iceland. In this paper we focus on data from three lava tubes in two distinct regions of Iceland during a PELE field expedition in the summer of 2018, during which we collected samples of microbial mats and their geological substrates. We obtained *in situ* elemental data with a portable X-ray fluorescence (XRF) spectrometer, analyzed biological samples with 16S rRNA gene sequencing methods, biogeochemical samples with Raman spectroscopy, and geological samples with scanning electron microscopy (SEM) and energy-dispersive X-ray spectroscopy (EDS). In synergizing these data sets, we attempted to describe the biogeochemical fingerprints of microbial life in lava tubes and define

their validity as biosignatures. While the microbial mats collected in the caves we visited came in a variety of colors, the blue samples are used here as a case study to exemplify our protocols, describe our workflow, and show the data that can be gleaned from such a study.

2 Materials and Methods

To gain a better understanding of what kinds of microbes thrive in oligotrophic, subterranean environments and the traces they leave behind, we analyzed an interdisciplinary set of samples collected in Icelandic lava tubes. Lava tubes are isolated, fragile, and potentially dangerous environments, and as such their exploration requires much care, planning, and specialized equipment.

2.1 Icelandic lava tubes

During a field expedition in the summer of 2018, we explored four lava tubes in two distinct regions of Iceland: the southern Eldhraun lava field and the northern Ódáahraun lava field. The caves, marked with black stars on Figure 1, are labeled B and C in the Eldhraun lava field (basaltic, intermediate, and acidic lavas since 1100 AD), and H and R in the Ódáahraun lava field (basaltic, intermediate, and acidic lava flows older than 1100 AD). The moss-covered Eldhraun lava field is part of the Laki lava flow originating from the Laki (Skaftfir Fires) fissure eruption in southern Iceland near the older Mt. Laki hyaloclastite formation during 1783 and 1784. The eruption produced 14.7 $\pm$ 1.0 km^3 of basaltic lava flow, with 2.6% of the erupted volume in the form of tephra and ash (Thordarson & Self, 1993). The Ódáahraun lava field is a sandy lava desert 5 000 km^{2}in size, composed of many older lava flows sometimes covered by recent pumice deposits (Sheth, 2018). The oldest lava flow originated 10-12 thousand years ago, and the youngest lava flow is from the Holuhraun eruption in 2014-2015 (Hannesdóttir et al., 2010). Within this huge expanse sits Mt. Herubrei, a classic table mountain, with hyaloclastite formations under its lava cap. Countless lava tubes abound in the Eldhraun and Ódáahraun lava fields, many of which have been explored by the Icelandic Speleological Society (ISS), who have noted and archived their locations, and worked extensively to keep them pristine and protected from human contamination.

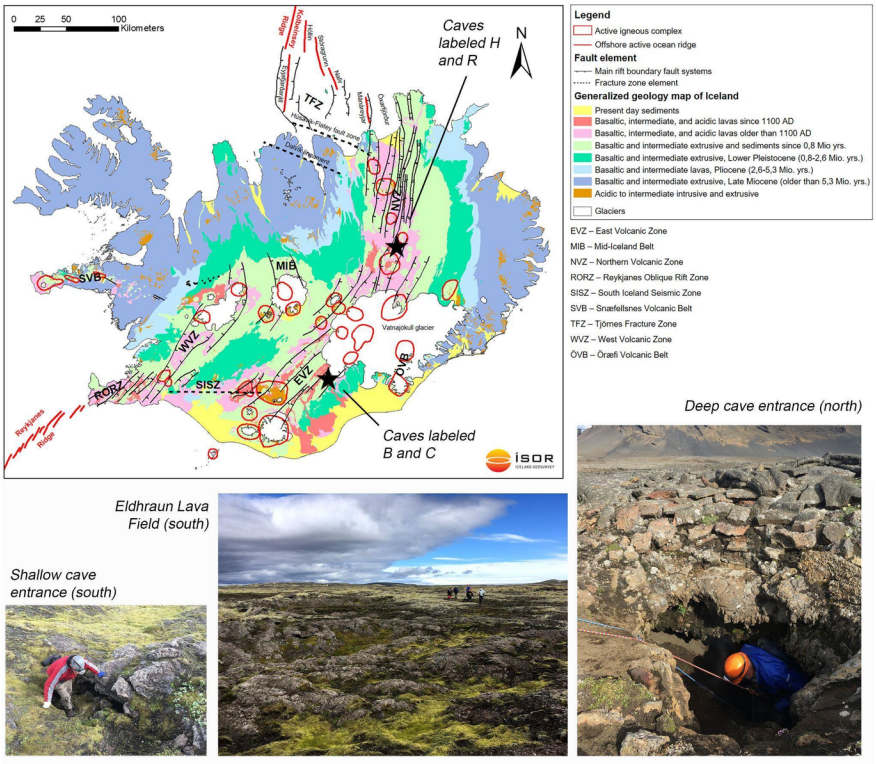

Figure 1. (top) Geological map of Iceland with black stars marking approximate cave locations. Map projection is ISN93. Courtesy of Anett Blischke, Icelandic GeoSurvey. **(bottom)** Lava fields visited and examples of cave entrances.

The Icelandic caves play host to a variety of microbial communities, as seen by microbial mats scattered across the cave ceilings, walls, and floors in all colors of the rainbow. Although the lava tubes themselves originate from relatively young flows (Figure 1), they also show some secondary mineral alteration. What is microbial mat and what is secondary mineral can often be difficult to distinguish, as their textures and colors can be interchangeable to the naked eye, and is compounded by the knowledge that they may be intricately linked.

Blue-colored mats/mineral precipitates observed in Icelandic lava tubes were often found on surfaces of flowing water or along cracks in cave walls or ceilings, where water seeps in from the ground above (Figure 2). Some blue features had a viscous texture (Figure 2b), while others were brittle mineral crusts attached to the lava rock beneath (Figure 2a). The blue features found in caves B, C, and H (Figure 4) are the subject of this paper, as well as a detailed account of their acquisition in an effort to inform the search for biosignatures in future missions to lava caves on Mars.

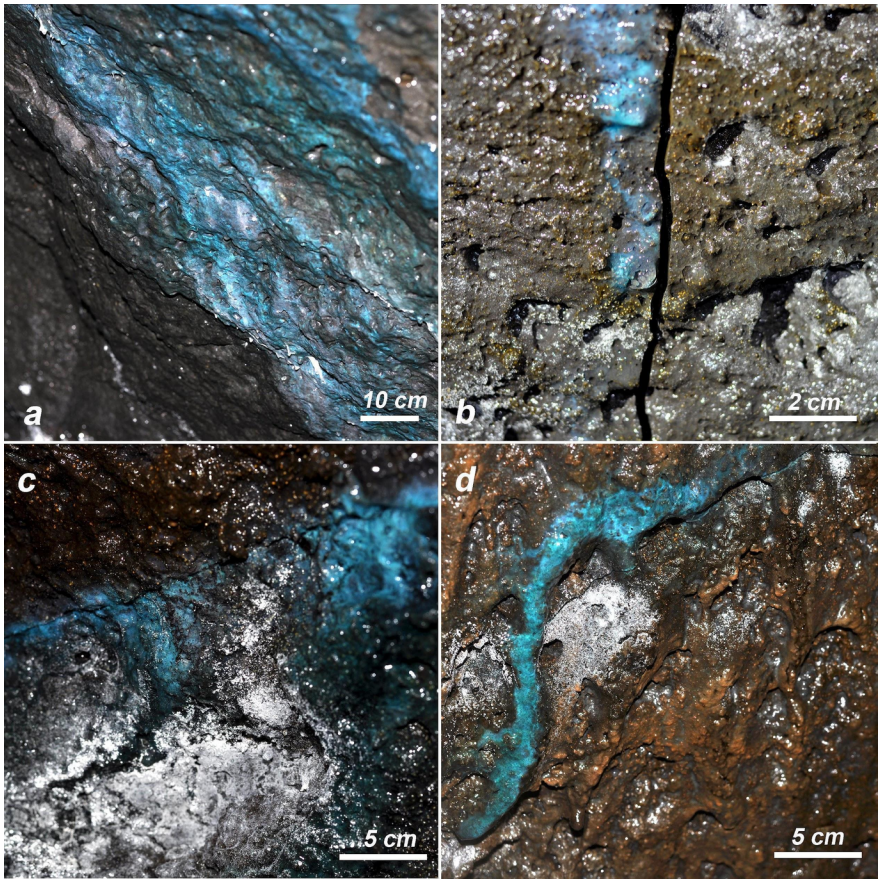

Figure 2 . Examples of blue features. Blue mats and mineral precipitates are often found on surfaces of flowing water **(a)** , or along cracks in cave walls or ceiling, where water seeps in from the ground above **(b-d)** .

2.2 Sampling strategy

Sampling sites were kept minimal in size, with great care taken to touch as little of the cave walls as possible, so as not to disturb or contaminate the microbial mats, which have a slow growth rate due to the environmental conditions and nutrient availability, taking several decades to reach macroscopic size. Speleothems, which form on geological timescales, are frequently vandalized, for example, the breaking of stalactites and stalagmites for personal collections and home decoration. Though sometimes unavoidable when sampling, such as when bumping the ceiling or walls in tight spaces, great care was taken to minimize damage of the mineral formations.

Initial training by cave connoisseur Diana Northup at a summer school in 2016 in the Azores organized by the European Astrobiology Campus, followed by several expeditions with the same core team honed the following 5-step sampling strategy (see also Figure 3).

Step 1. Trace gas analysis, performed by one person to measure CO_2, SO_2,NH_3, H_2S and NO_x, which have the potential to be dangerously high in caves.

Step 2. Microbial mat sampling, by scraping the mat off the rock under sterile conditions for DNA extraction and 16S rRNA gene sequencing analysis.

Step 3. Biogeochemical sampling, by chipping away a section of mat-covered rock with a geological hammer under sterile conditions for molecular analysis.

Step 4. Recording of the elemental composition of the rock below the scraped mats using a handheld XRF spectrometer.

Step 5. Geological sampling by chipping away the surface rock with a geological hammer for mineralogical analysis.

Figure 3. Sampling strategy. **(a)** Cave entrance to cave H, 12 m below ground. **(b)** Sampling in pairs: one sampler and one assistant handling cleaning and handing over of tools. **(c)**Biological sampling (step 2): scraping mats from the cave wall.**(d)** Handheld XRF measurements of cave wall (step 4).**(e)** Substrate sampling with a geological hammer and Falcon tube (steps 3 and 5).

2.2.1 Biomass sampling for DNA analysis

In order to minimize contamination, the second step in the sampling technique (after step one: ensuring the team's safety with the trace gas analyzer) was the collection of biomass for DNA extraction and sequencing (Figure 3c). Sampling began by sterilizing sample tools, i.e. scoops and spatulas with cleaning acetone and 70% ethanol, eliminating potential organic contaminants. We wore nitrile gloves washed with 70% ethanol, and used scoops and sterile Eppendorf tubes to scrape the surface of the lava tube to collect the overlying biomass. The sampling was best done with two people, one doing the sampling and one assisting with cleaning and in handing over tools and sampling tubes (Figure 3b). Samples were collected in biological triplicate to ensure enough samples for any repeated analyses. Samples were then stored at 4°C onsite and for shipment and finally at -20°C until the DNA extraction protocol began.

2.2.2. Biogeochemical sampling for molecular analysis

The third step in sampling was the collection of geological samples covered in biomass. We sterilized tools using the same acetone and 70% ethanol-based sterilization technique as for DNA sampling and used sterile 50 mL Falcon tubes to catch the biomass-covered rock samples that we chipped off with the hammer, which was flame sterilized with a lighter in addition to the solvent cleaning (Figure 3e). Collected in triplicate, these samples were also stored at 4°C to ensure minimal alteration of biomolecules.

2.2.3 Portable X-ray Fluorescence (XRF)

A portable NitonTM XL3t GOLDD+ X-Ray Fluorescence Analyzer from Thermo Fischer gave us elemental data *in situ* (step 4). It can detect up to 30 elements from Mg to Bi in the standard range without helium or vacuum assistance. The measured concentration of the sample must be at least three times the standard

deviation of the measurement (i.e., detection limit); the measurement confidence is 95% (two sigma). "Mining mode" (best for analyzing raw or semi-processed mineral samples of varying density) was used for elemental quantification. The instrument was placed against the cave wall, measuring both the biofilm substrate post biological sampling as well as nearby uncolonized locations with an analysis time of 90 seconds.

2.2.4 Geological sampling of the lava tube substrate

Geological sampling was the fifth and final step in the sampling protocol. We chipped off rock samples from the cave wall with a geological hammer and stored them in ziplock bags under ambient conditions. The samples were then analyzed with SEM/EDS.

2.3 Characterization of microbial samples

To obtain phylogenetic data we performed DNA extractions, PCR amplification, and genetic sequencing on the microbial samples collected in step 2 of the sampling procedure.

2.3.1 DNA extractions Genomic DNA was extracted in triplicate from the biofilm samples using a method previously used with environmental rock samples with phototrophic communities (Stivaletta et al., 2012). First a washing step was performed, wherein 200 µL (or weight equivalent ˜200 mg) of the samples were resuspended in 1.5 mL of TE pH 8 (10 mM Tris Hydrochloride pH7.4 + 1mM EDTA pH 8), centrifuged at 10000 rpm for 10 min, after which the supernatant was discarded, and the pellets resuspended in 400 µL of TE pH 8. Then, the solution was added to sterile tubes with glass beads (Lysing Matrix tubes, MP Biomedicals, 1.4 mm ceramic beads, 0.1 mm silica spheres and one 0.4 mm glass sphere) and subjected to a bead beater two times 60 s at 6 m/s (MP Biomedicals, FastPrep24). Subsequently, 300 µL of phenol saturated with 0.1 M Tris Hydrochloride (tris-phenol, pH 7.4) and 300 µL of chloroform/isoamyl alcohol (24:1) were added to the tubes, and subjected to three 2-min cycles of heating at 60°C and vortexing for 30 s. After centrifugation (10 000 rpm, 5 min) the aqueous phase was extracted once with tris–phenol/chloroform/isoamyl alcohol (25:24:1); then 1/5 volume of TE buffer was added, and the pellet extracted again with phenol. Finally, the aqueous phases were extracted with chloroform/isoamyl alcohol (24:1) and nucleic acids precipitated overnight at -20°C with cold absolute ethanol and 0.3 M sodium acetate. After centrifugation (10 000 rpm, 5 min) and washing with 1 mL cold (-20°C) 75% ethanol, the pellets were dried out and resuspended in 30 µL nuclease free water. 2.3.2 PCR Amplification, Library Preparation and Sequencing

PCR amplification was made with PuRe Taq Ready-To-Go PCR Beads (GE Healthcare), 1 µL of each Illumina barcoded forward and reverse primers (16S rRNA gene V4 region primers 515F: GTGBCAGCMGCCGCGGTAA and 805R: GACTACHVGGGTATCTAATCC), 2 µL of DNA template, and 21 µL of nuclease-free water. The PCR cycling program used was 98°C for 30 s (denaturation), 35 cycles of 10 s at 98°C, 30 s at 60°C, 4s at 72°C, and 2 min at 72°C.

The multiplexed amplicon library was prepared by pooling equal amounts (20 ng) of each sample and paired-end sequencing was performed (at the SNP&SEQ Technology Platform, SciLife Labs, Sweden) on Illumina MiSeq with 300 base pairs (bp) read length using v3 sequencing chemistry. Raw sequences were processed with the R package DADA2 (version 1.18.0) (Callahan, Mcmurdie, et al., 2016). Due to low quality reverse reads affecting the merging of paired ends, we only used forward reads in the downstream analysis. Reads were truncated to 220 bp and assigned taxonomy using the Silva_132 database (Quast et al., 2013) and the RDP naïve Bayesian classifier (Wang et al., 2007). ASVs (Amplicon Sequence Variants) were normalized by Cumulative Sum Scaling. All samples with less than 100 reads were excluded from the analysis, and biological triplicate samples were merged. Visualization was done using the R packages phyloseq (v1.34.0) (McMurdie & Holmes, 2013) and ggplot2 (Wickham, 2016), and Krona plots were made with Krona (Ondov et al., 2011).

2.4 Characterization of geochemical and geological samples

To characterize the geological substrate and identify any molecular biomarkers therein, we analyzed the geochemical samples collected in step 3 using confocal Raman microscopy and the geological samples collected in step 5 using SEM/EDS. The geochemical samples were first pulverized with a mortar and pestle under

sterile conditions. The geological samples were polished into thin sections without any prior treatment and coated with platinum or carbon (when carbon content was not analyzed).

2.4.1 Confocal Raman microscopy

Raman spectra were obtained with a confocal WITec alpha 300 system, at the DLR Berlin, consisting of a microscope equipped with a 10x long working distance objective with a 0.25 numerical aperture, a piezo-driven scan table, a UHTS 300 spectrometer with an ultrafast EMCCD detector and a frequency-doubled Nd:YAG laser. The excitation wavelength of the laser was 532 nm, the spot diameter at the sample was ˜2.5 µm and the spectral resolution of the spectrometer was 4-5 cm^{-1}. Integration time and laser power were varied according to the investigated sample (1-10 s and 0.1-7 mW respectively) to produce spectra with a sufficient signal-to-noise ratio, and to prevent sample damage/degradation and detector saturation. 2.4.2 SEM/EDS analysis of thin sections Secondary electron (SE) and backscattered electron (BSE) images of platinum and carbon-coated thin sections were obtained using a Zeiss GeminiSEM 450 Field Emission Gun Scanning Electron Microscope at Utrecht University, using 10-20 keV accelerating voltage, a 250-1000 pA probe current, and a 10 mm working distance. The SEM was coupled with a windowless Oxford Instruments Ultim-Extreme EDS detector to characterize the elemental composition of the minerals present in the thin sections. Overview element distribution maps (15-60 min counting time) and point ID measurements (30 s counting time) were acquired at voltage of 20 keV and 1 nA, using Oxford Instruments Aztec software v5.1. For improved spatial chemical resolution in finely zoned domains, an accelerating voltage of 10 keV was used, acquiring the L-alpha intensity of Cu.**3 Results**To investigate cave biosignatures, we carried out fieldwork in Icelandic lava tubes, where we collected biological, biogeochemical, and geological samples, and *in situ* elemental data using a multi-step sampling protocol. We then characterized the samples using a variety of analytical techniques. Here we describe the results in sections based on the location of the collected samples, the type of sample, and the analytical technique used. 3.1 Surface & subsurface field observations 3.1.1 Sampling sites

The caves sampled include caves B and C in the southern Eldhraun lava field, and H and R in the northern Ódáahraun lava field (Figure 1). The lava rock in the caves visited appears largely unaltered, and the presence of microbial mats is much scarcer than that seen by our team and others (Hathaway et al., 2014) in lava tubes in the Azores. Still, we observed alteration minerals and microbial mats of various, striking colors.

The cave entrances in the southern Eldhraun lava field are very shallow, and the entirety of the tubes is no more than two meters below the surface. The temperature was measured at 8°C, and much water condensation was observed on the cave walls, of which we measured a pH of 8.1 near the sampling sites. In cave B we observed white, red, yellow, and blue mats on top of the cave walls, while in cave C we found green, blue, red, and white mats. The cave entrance to cave H in the Ódáahraun lava field was twelve meters below the surface, requiring four connected three-meter-long ladders, and additional propelling equipment for the team as a failsafe. The entrance of cave R was equally deep, but accessible by foot down a steep ash mound. Compared to the southern caves, the temperature in the northern caves was colder, measured at 3°C, the cave ceilings were higher, and the walls generally appeared much drier. We observed many blue and purple mats, orange and yellow mats, grey slime, black dots, and fluffy white deposits on the cave walls. While most microbial mats seemed to be randomly dispersed on the cave walls, the blue precipitates occurred only where water was present, such as along cracks in the cave walls (Figure 3). 3.1.2 Samples collected

A variety of mat colors were sampled, including white, yellow, orange, grey, purple, and blue. The blue mats were distinct from the others in their incredible vibrancy of color, and in their consistent occurrence in places of flowing water, near cracks in the cave wall or ceiling, or in puddles on the ground. Blue mat and rock samples were collected in caves B, C, and H (Figure 4). Blue features were found surrounding a crack in cave B (Figure 4a), on a water droplet on a ceiling in cave C (4b), and at two sample sites in cave H, one on the wall (4c) and one in a puddle on the ground (4d). While the puddle in Figure 4d was very wet, offering up a wealth of viscous material for biological sampling, not all of the sampling locations were so generous. The blue material on the cave wall in Figure 4c was fused to the rock and had to be scraped off with much patience.

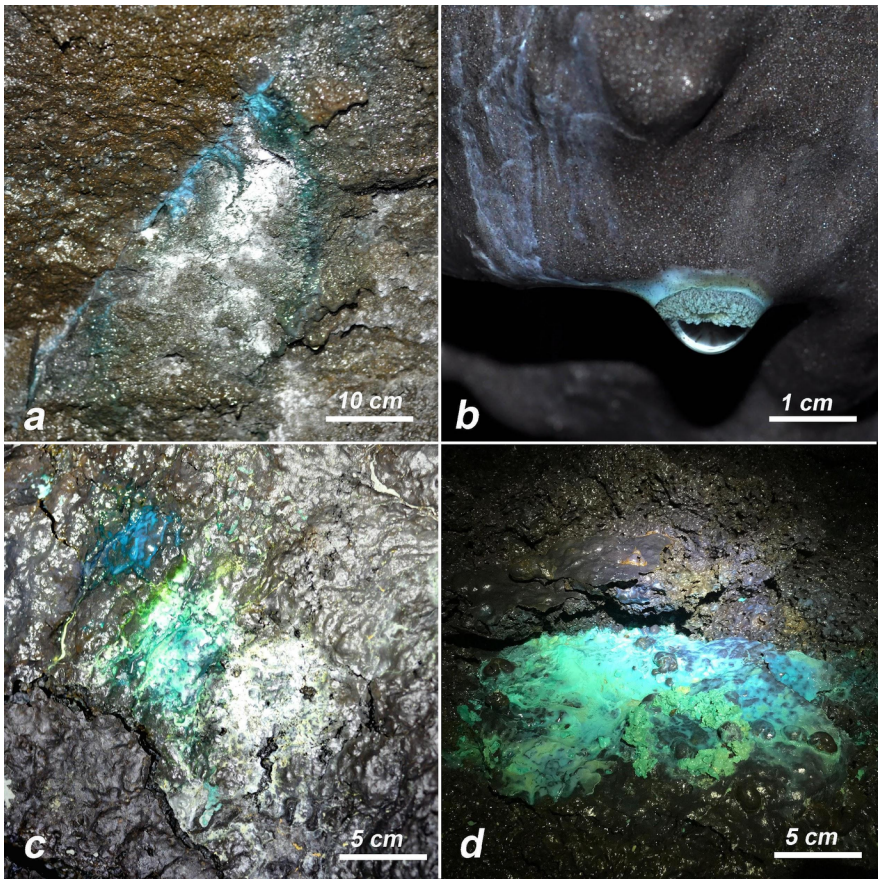

Figure 4. Sampling sites of blue features. **(a)** Sample B5 from cave B. **(b)** Sample C2 from cave C. **(c)** Sample H1 from cave H. **(d)** Sample H7 from cave H.

3.2 Blue Sample Analysis

Blue features were found to have prominent copper enrichments with our portable XRF while sampling them. We thus grouped these into one study and analyzed them further with 16S rRNA gene sequencing methods, Raman spectroscopy, and SEM/EDS in an attempt to understand the cause for such high concentrations of copper in an environment where it is expected to be scarce. The analyses performed on each sample can be seen in Table 1.

Cave Name	Sample	Analyses Performed	Relevant Figures
B (south)	B5	SEM/EDS	4a, 9
C (south)	C2	XRF, 16S rRNA sequencing, Raman	4b, 5c, 6a-f, 8
H (north)	H1	XRF	4c, 5a-c
H (north)	H7	XRF, 16s rRNA sequencing, SEM/EDS	4d, 5c, 6a-d, 7, 10

Table 1. Overview of blue samples and analyses performed.

3.2.1 X-Ray Fluorescence XRF analysis of sample H1 (Table 1) of the mat substrate versus the background (collected from a region close to the sampling spot not covered by mat) revealed several differences between the elements present. Iron, calcium, silicon, magnesium, titanium, and manganese were decreased in mat substrate samples as compared to the background, while copper, phosphorus, and aluminum were lower in

the background and higher in the mat-covered samples (Figure 5a). The mat substrate samples showed a striking enrichment in copper, which given the amount of aluminum and silicon present, could be in the form of a hydrated copper silicate. The Al:Cu:Si ratio of the mat substrate versus the background is shown in Figure 5b.**Figure 5.** XRF measurements of blue precipitates in sample H1 vs. background. **(a)** Major elements were measured by pointing the XRF onto the cave wall where the mat was collected, vs. the background, i.e., a spot on the wall nearby not covered in mat.**(b)** Ratios of select elements aluminum, copper, and silicon in blue precipitate vs. background. Copper is markedly absent in the background. **(c)** Al:Cu:Si ratios measured in all blue precipitates. Figure 5c shows the Al:Cu:Si ratio of samples C2 (0.33:3.3:1), H1a (0.81:0.35:1), H1b (0.73:0.29:1), H7a (0:12.8:1) and H7b (0.07:1.6:1). A typical Al:Cu:Si ratio of chrysocolla, an amorphous, hydrated copper silicate, is 0.12:1.98:1 (Anthony, 1990), and is in the same range as samples C2 and H7b. 3.2.2 DNA sequencing Blue samples C2 (from cave C in southern Iceland) and H7 (from cave H in northern Iceland) were analyzed for bacterial community composition based on DNA extracted using phenol/chloroform with ethanol precipitation and amplified using V4-specific 16S rRNA gene primers (Figure 6). At the phylum level (Figure 6a, b), Proteobacteria strongly dominated the bacterial community composition. The most common family was Burkholderiaceae in both samples (Figure 6a, b). C2 and H7 contained a number of similar genera (Figure 6c), notably *Ralstonia*(Proteobacteria) *(*74% in C2 and 74% in H7) and*Caulobacter* (Proteobacteria) (20% in C2 and 5% in H7). The genera *Corynebacterium* (Actinobacteria), *Cutibacterium*(Actinobacteria)*,* and *H1* (Bacteroidetes) were only found in sample C2, while *Cupriavidus* (Proteobacteria)*,Methylobacterium-Methylorubrum* (Proteobacteria), and*Thermovirga* (Synergistaceae) were found exclusively in sample H7. No archaeal 16S rRNA sequences were detected.

3.2.3 Confocal Raman Spectroscopy

Sample C2 in Cave C was analyzed using confocal Raman spectroscopy. A drop of water hanging from the ceiling containing a significant amount of blue precipitate was observed under the microscope and identified with brown speckles incorporated in the crystalline deposit (Figure 6d). The Raman spectrum of the brown speckle shows prominent peaks at 1008, 1155, and 1513 cm^{-1}, typical of a carotenoid signature (Figure 6e). The 1008 cm^{-1} peak corresponds to the in-plane rocking modes of the CH_3 groups attached to the polyene chain, while the peak at 1155 cm^{-1} is associated with C-C stretching and C-H deformation, and the one at 1516 cm^{-1} with C=C stretching (Vítek et al., 2009; Baqué et al., 2018).

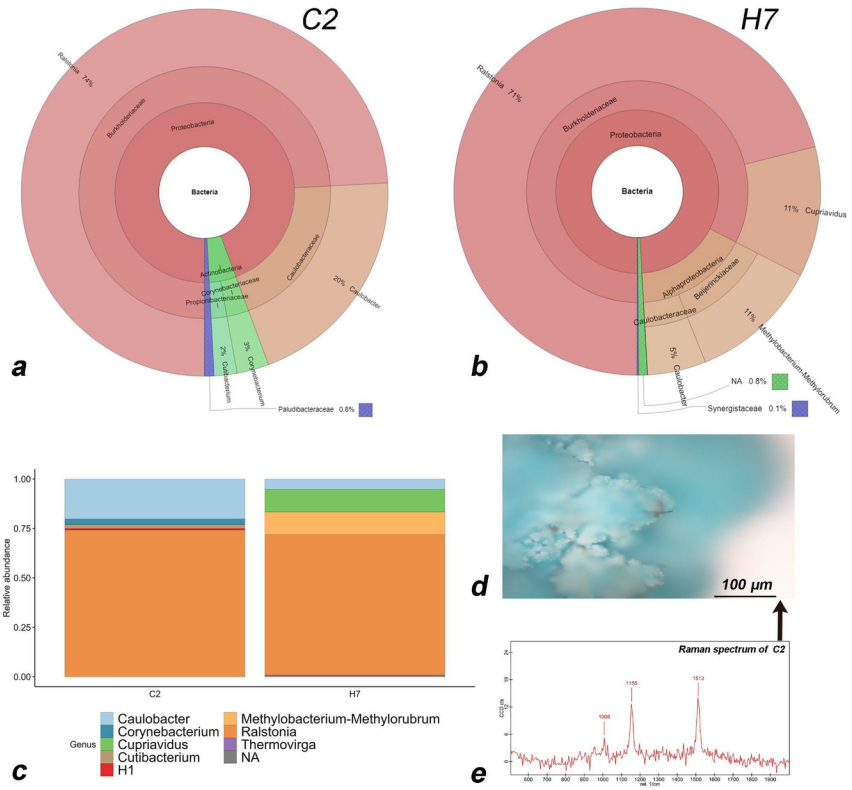

Figure 6. DNA sequencing and Raman spectroscopy results.**(a)** Krona plot of C2 showing relative abundances of Phyla, Classes, Orders, Families and Genera. **(b)** Krona plot of H7.**(c)** Bar plot showing relative abundance of genera of C2 and H7.**(d)** Optical microscopy image of blue drop material (sample C2) with visible brown speckles. **(e)** Raman spectrum of brown speckle inside blue drop material, with prominent peaks at 1008, 1155, and 1513 cm^{-1} typical of a carotenoid signature.

3.2.4 SEM/EDS analysis of thin sections Figure 7 shows a comprehensive summary of the igneous minerals of the lava rock in the sample H7 thin section. The lava rock is composed of unaltered basalt, as seen from the pristine and angular grain boundaries. The igneous mineralogy consists mainly of clinopyroxene, ilmenite, and plagioclase. Igneous titano-magnetite has exsolved into Ti-poor magnetite and ilmenite. Phosphorus enrichment in tiny crystals in interstitial melt pockets suggests apatite saturation, in agreement with a highly evolved residual melt composition left after high degrees of crystallization.

Figure 7. Igneous mineralogy. **(a-c)** Backscattered electron (BSE) images of sample H7 thin section, showing clear, angular grains indicating largely unaltered basalt. **(c)** EDS point spectra taken of spots marked in red, revealing typical basaltic mineralogy: augitic clinopyroxene (2), dendritic titano-magnetite, (oxy-) exsolved into a fine intergrowth of Ti-poor magnetite (white) and ilmenite (slightly less bright) (4), plagioclase (5), magnetite (8), and apatite growth, indicating a highly evolved interstitial melt pocket (10). The spectra can be seen in Supporting Information.

Upon closer inspection of the thin section edges, surfaces potentially exposed to microbial mats, we see a ˜10 µm thick secondary mineral crust with a botryoidal, layered appearance in sample C2 (Figure 8a, b). It shows many fractures and damage, and is only sporadically present, suggesting it is fragile and not well-preserved in the sample handling and thin section preparation process. It also appears to have been deposited on top of the igneous rock, rather than leached from it, based on the clear boundary between the two and the independent growth pattern of the precipitate.

Another location in sample C2 with the secondary mineral crust was found and mapped with EDS (Figure 8c). The EDS spectrum in Figure 8i shows an augitic clinopyroxene as an igneous phase of the parent lava rock, which forms a sharp, unaltered boundary to the Ca-free crust (Figure 8e). The EDS spectrum of the crust (Figure 8h) shows a prominent copper enrichment, along with aluminum and silicon, and minor sulfur. The element maps shown in Figures 8f and 8g indicate that the copper enrichment in the crust is associated with uniformly high aluminum intensities. In addition, the crust material was observed to form shrinkage cracks under high vacuum and exposure to the (low-current) electron beam, consistent with a hydrous mineralogy. This resembles the signature of the hydrated copper silicate chrysocolla (Anthony, 1990), supported by the botryoidal, blue appearance. The crust has uniform, percent-level phosphorus concentrations.

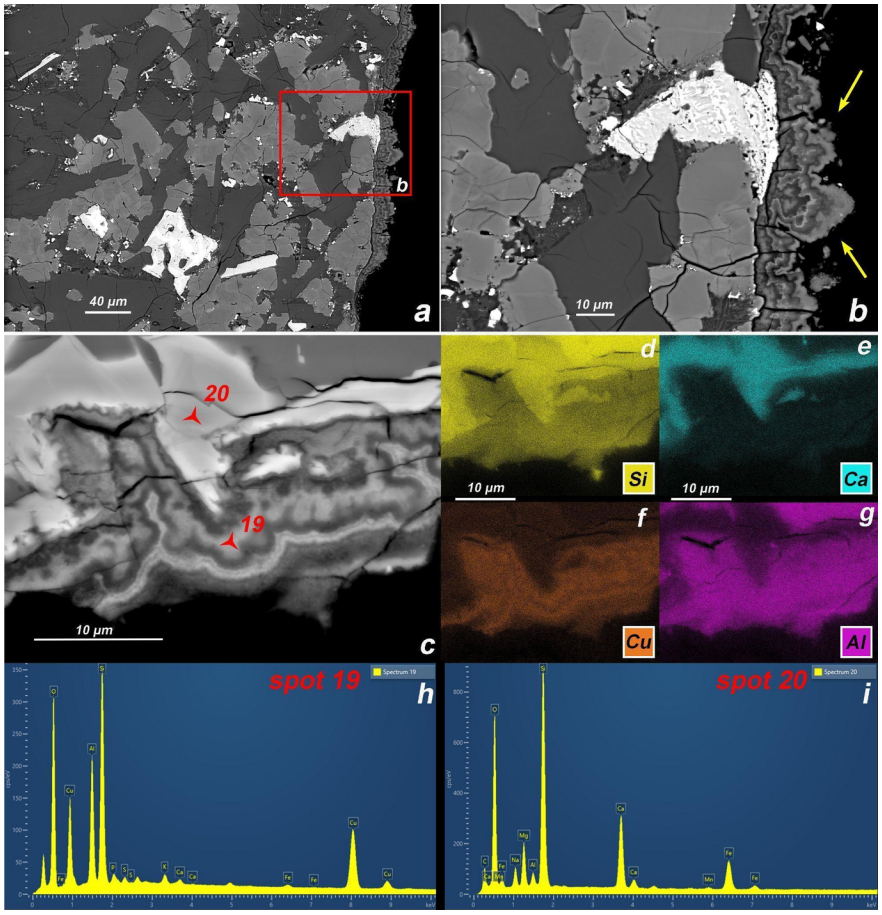

Figure 8. Botryoidal secondary mineral precipitate.**(a)** BSE image of a botryoidal, layered secondary mineral crust deposited on the edge of the igneous rock in sample C2. **(b)**Zoom-in on botryoidal crust, indicated by the yellow arrows.**(c)** BSE image of the botryoidal mineral crust in another location in C2. **(d-g)** Elemental maps of silicon, calcium, copper, and aluminum present in the section presented in (c).**(h)** EDS spectrum of spot 19 (secondary mineral, pane c), showing copper and aluminum enrichment, possibly indicative of chrysocolla. **(i)** EDS spectrum of spot 20 (lava rock, pane c), showing unaltered augitic pyroxene.

In sample B5 from Cave B, we observed a more complex secondary mineral precipitate, with additional elemental enrichments and more discrete layering (Figure 9). This precipitate was not as botryoidal in appearance as that of sample C2, but was also enriched in copper and displayed distinct layering when

mapped with EDS. It is clear that the copper occurs in the entirety of the deposit alongside all other elements (Figure 9f), however the amount of aluminum it is associated with varies in the different layers (Figure 9g). Additionally, there is a manganese-enriched layer that occurs in a silicon- and aluminum-poor region, as seen when comparing Figures 9e to 9d and 9g.

We were able to better distinguish the distribution of elements in the precipitate by mapping a small area with an excitation voltage of 10 keV for better spatial resolution of elements (Figure 9h). The EDS map sum spectrum in Figure 9m shows copper, aluminum, manganese, and phosphorus enrichments. The elemental maps confirm that manganese occurs in silicon-poor regions (Figure 9i) and that manganese and aluminum are competing (Figure 9j). Comparing Figure 9j to 9i and 9k, it is evident phosphorus enrichment occurs in silicon-poor regions, suggesting discrete phosphate minerals that contain copper. The outer layer of the complex crust is carbonate-bearing, as seen by the increased carbon level in the elemental map in Figure 9l, distinctly separate from the strong carbon signal produced by the epoxy above it.

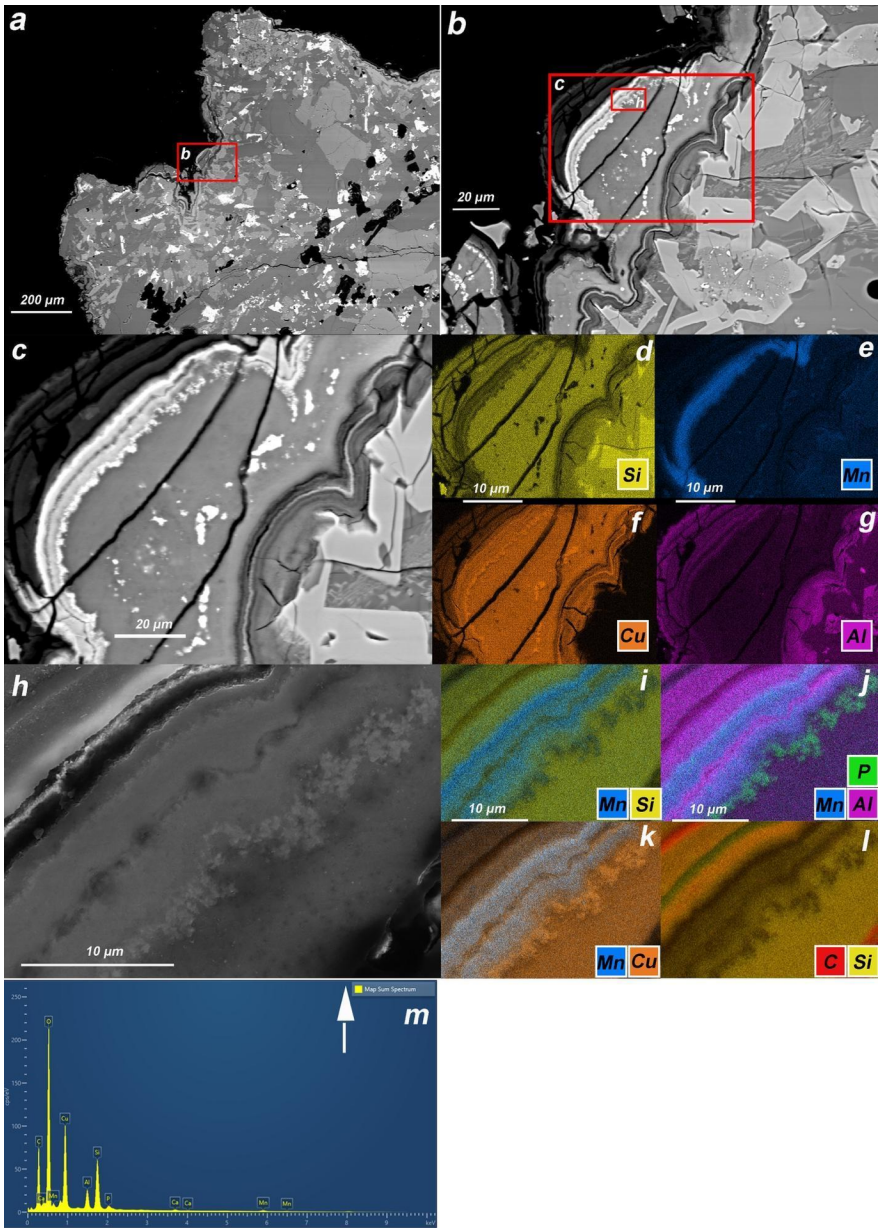

Figure 9. Complex secondary mineral precipitate. **(a-c)**BSE image of a secondary mineral crust deposited on the edge of the igneous rock in sample B5 thin section. **(d-g)** Elemental maps of silicon, manganese, copper, and aluminum. **(h)** BSE image of close-up of secondary mineral crust. **(i-l)** Composite elemental maps of manganese and silicon **(i)** , phosphorus, manganese, and aluminum **(j)** , manganese and copper **(k)** , and carbon and silicon **(l)** . **(m)** EDS sum spectrum of (h) showing copper, phosphorus, and manganese enrichment. The EDS sum spectrum of (c) can be seen in Supporting Information.

These elemental maps suggest that a variety of minerals are precipitating alongside each other in the complex secondary mineral precipitate in Figure 9c, starting with an aluminum-poor copper silicate on the bottom right, followed by a copper phosphate, a manganese oxide or hydroxide, an aluminum-rich copper silicate, and topped off with a carbonate-bearing layer. The aluminum-rich copper silicate may be chrysocolla as discussed in previous sections. Pseudomalachite could be a candidate for the copper phosphate species based

on the elemental distribution, and that it is similar in outward appearance and known to be associated with chrysocolla.

4 Discussion

We first gave a thorough description of our workflow in the field, explaining how we approach subterranean Martian analogue environments in search for biosignatures. We then presented a case study of blue microbial mats and their substrates from three lava tubes in Iceland analyzed with a variety of analytical techniques, namely a portable XRF, 16S rRNA gene sequencing, Raman spectroscopy, and SEM/EDS. Here we discuss the possible origins of the copper-rich secondary mineral precipitates, the significance of the bacteria that inhabit them, and the molecular markers they leave behind therein.

4.1 Cave geology and speleothems

We observed stark differences in elemental concentration (with preliminary *in situ* XRF readings) between the substrates where the microbial mats were sampled and the background areas, i.e., uncolonized areas nearby the sampling locations (Figure 5a-c). This demonstrates an altered geological substrate that biofilms either contribute to or benefit from in order to thrive in this environment. Our mineralogical and elemental analysis of the lava rock substrate (Figure 7) and blue secondary mineral precipitates (Figures 8-10) show sequestering of elements more generally dispersed and scarce in basaltic lava tubes, particularly copper. The boundaries between the unaltered basalt and the precipitate rim, as seen in the SEM images of the thin sections (Figures 8 & 9), are pristine, dictating that the elements that make up the observed blue mineral precipitates must have filtered in with the water through cracks in the cave walls or ceiling, instead of being leached from the host rock.

4.1.1 Sources of copper in Iceland

The average copper content of recent Icelandic basaltic lava is low, in the range of 10-200 ppm (μg/g) (Eason & Sinton, 2009; Gibson et al., 1982), with occasional higher values found in older Miocene volcaniclastic rocks (Schmincke et al., 1982). Similarly, the copper content of Icelandic groundwater is also low, ranging from 0.00015 to 0.00209 ppm (Gunnarsdottir et al., 2015) where the Cu(II) ion is the more common oxidation state (Schock et al., 1995). However, copper is a semi-volatile element that can partition into a volatile-rich fluid that can physically separate from magma (Candela & Holland, 1984). Copper has been observed to be enriched in volcanic laze plumes from basaltic intraplate volcanoes, which can transfer it directly into the marine biosphere (Mason et al., 2021), and result in highly copper-enriched groundwater in specific areas. In the case of Iceland, copper is enriched in hyaloclastite deposits at the lava-ice interface (Furnes, 1978) and from there could be readily mobilized into groundwater that can infiltrate the lava tubes through cracks. In addition, rain and melting snow could be leaching copper from the volcanic ash that abounds on the lava fields above, bringing it into the tubes through cracks and cave openings. Kiernan et al. (2003) has noted the hydrogeological significance of lava tubes in the Eldhraun lava field, with rainwater and floods transporting glacio-aeolian deposits in these efficient groundwater flow channels.

Volcanic ash, derived from explosive eruptions of evolved intermediate-silicic volcanoes, has an evolved nature relative to basaltic lava flows, characterized by an enrichment in many incompatible elements, including copper. Hoffmann et al. (2012) showed that copper was released from various volcanic ash samples in concentrations up to 0.00065 ppm after just 15 min of contact with seawater. Smith et al. (1982) reported an average concentration of 0.39 ppm of Cu in leachates from volcanic ash in experiments simulating its interaction with rainfall and prolonged exposure with groundwater. Experiments with volcanic ash from the 2000 eruption of the Mt. Hekla volcano in Iceland showed a Cu flux of 0.069 ppm within 8 hours of mixing with deionized water (Jones & Gislason, 2008). Though this eruption would not have reached our areas of interest at the initial deposition stage, the volcanic cloud spewed out 0.1 Tg of ash (Rose et al., 2003), allowing it to be transported north-northeast by wind and depositing up to 5 kg/m^2 on the headwaters of the Ytri–Rangá River (Haraldsson, 2001).

There could thus exist many sources of copper in the Ódáahraun and Eldhraun lava fields, including the

hyaloclastite formations in nearby Mt. Laki and Mt. Herubrei. The precise source of ash in the Ódáahraun lava field is difficult to determine, as wind plays a large role in transportation of ash and sand, and a large proportion of it (some of which may be copper-rich ash and shattered hyaloclastite material) has been blown long distances over the lavas from sources closer to Vatnajökull glacier or the Jökulsá á Fjöllum glacial river (Arnalds, 2015). Indeed both the Ódáahraun and Eldhraun lava fields are subject to severe wind erosion and very high aeolian deposition rates (Arnalds, 2010; Arnalds et al., 2001), constantly replenishing the areas with volcanic ash.

4.1.2 Copper abundance on Mars

The surface of Mars is enriched in sulfur (Rudnick & Gao, 2003), and is thus expected to show elevated concentrations of chalcophile elements such as copper in the crust (Payré et al., 2019). Copper abundance values up to 580 ppm were detected by the Curiosity rover in the Liga sedimentary bedrock at Gale Crater (Berger et al., 2017). A chrysocolla bearing unit, along with pseudomalachite and other copper mineral phases, has been identified in the Shalbatana Valley palaeolacustrine system on Mars, and is hypothesized to be a supergene alteration product of copper sulfide minerals interacting with oxygen and water (Popa et al., 2014). This indicates a redox system capable of oxidizing Cu^{+} to Cu^{2+} in an oxidizing environment in Mars' past, which would likely have extended to lava tubes. Copper enrichments seemingly precipitated from groundwater have been found adsorbed to manganese deposits in the Kimberley Formation in Gale Crater on Mars, and are thought to be deposited in oxidizing conditions within fractures in the bedrock (Payré et al., 2019).

4.1.2 Blue speleothems in Iceland

In Figures 8-10 we described copper-rich secondary mineral precipitates as elucidated by SEM/EDS. While Figure 8 and 10 show a single copper phase, Figure 9 boasts a more complex precipitate, with discrete layers of copper silicates, copper phosphates, manganese oxides, and carbonate-bearing species. The copper phases present are expected to be mostly in the Cu(II) oxidation state, as this is the ion more readily available in the groundwater (Schock et al., 1995), and because of the prominent blue color (Cu(I) minerals are generally red/brown). Chrysocolla, an amorphous copper phyllosilicate, was found in samples C2 (Figure 8), B5 (Figure 9), and H7 (Figure 10). A similar finding was previously reported in lava tubes in Kipuka Kanohina Cave Preserve in Hawai'i by Northup et al. (2011), who also found a blue drop filled with a precipitate with an Al:Cu:Si ratio of 0.15:1.8:1 as analyzed by EDS, comparable to a typical chrysocolla ratio of 0.12:1.96:1 (Anthony, 1990). We also identified a layer of pseudomalachite in sample B5, which has been hinted at often being associated with microbial mats (Little & Wagner, 2018). Manganese oxides can be deposited by microbes in waters with manganese concentration as low as 10-20 ppb (Dickinson et al., 1996). Manganese oxidation is associated with the metabolism of several genera of bacteria. *Leptothrix* (a Proteobacteria associated with strictly low concentrations of organic matter) has been shown to deposit amorphous MnO_2 (vernadite) and a black MnO_2 precipitate (birnessite) (Gounot, 1994), while*Bacillus* has been observed to recrystallize birnessite to octahedral Mn_3O_4 (hausmannite) (Nealson et al., 1988). Boston et al. (2001) found manganese oxides in limestone caves to be linked to biogenic activity, identifying biogenically precipitated manganese 'snow' in limestone caves using a suite of analyses, including culturing Mn-oxidizing bacteria isolated from the 'snow' and observing them produce amorphous manganese oxides in the laboratory. Ultimately, blue, copper-rich speleothems are attractive targets for astrobiological research, as they house bacterial communities resistant to elevated copper content. Should they occur in lava tubes on Mars, they could also be thought of as a biotope within the caves, host to extremophilic organisms. 4.2 Bacterial communities inhabiting blue mineral precipitates The bacteria found in copper-enriched areas in the caves are present there because they can tolerate such an environment, and they actively sequester and adsorb copper ions. The significance of the bacteria identified and their copper-coping mechanisms are discussed below. Proteobacteria was the major phylum identified in the blue samples in the southern cave (C2) and northern cave (H7). Families and genera were generally similar across the samples, with some notable deviations. Differences in environment (average cave temperature, age of lava tube, humidity, etc.) may contribute to the differences in bacteria present inside of the caves from north to south; however, there was a large overlap

in the major abundances found. A recent study (Selensky et al., 2021) suggests that surface environment is not a major factor in organic nutrient cycling in lava tubes, which further exemplifies them as isolated environments that may harbor chemolithoautotrophic organisms and biosignatures that are useful in the search for life in extraterrestrial lava tubes. Furthermore, Northup et al. (2016) found that bacterial diversity in Icelandic lava tubes differed substantially from that in surface soil samples, with the most abundant cave phylum being Actinobacteria, followed by Acidobacteria and Proteobacteria.

The majority of genera detected in the blue samples (C2 and H7) represent copper-resistant oligotrophs. *Ralstonia, Caulobacter, Cupriavidus,* and *Corynebacterium* accounted for 97% of the relative genus abundance in sample C2 (Figure 6a). In sample H7 *Ralstonia, Cupriavidus, Caulobacter,* and *Methylobacterium-Methylorubrum* accounted for a total of 99% of the relative abundance (Figure 6b). *Ralstonia, Caulobacter, Cupriavidus* , and *Corynebacterium* are reported to have high metal resistance, which explains their presence in high copper concentration regions of the caves (Janssen et al., 2010; Mergeay et al., 2015; Morosov et al., 2018; Yang et al., 2019). Copper is essential for bacteria in trace amounts as it is utilized as a micronutrient as well as an enzymatic cofactor for redox activities (Giachino & Waldron, 2020). Copper resistance is found in different mechanisms within the bacteria, the most ubiquitous being a) oxidation of Cu(I) to Cu(II), a less toxic ion to bacteria; b) copper sequestration by metallothioneins and c) transmembrane copper export (Ladomersky & Petris, 2015). Additionally, the genome of *Cupriavidus metallidurans* contains *cop* genes, which are highly induced by Cu(II) and encode for copper exporting P1B-type ATPases (Monchy et al., 2020), and *cueO* genes encoding for multicopper oxidase (Sanyal et al., 2020).

Much of the literature discusses the ability of both *Cupriavidus* and *Ralstonia* to adsorb metals to their cell membrane. Morphological changes can be seen as they adjust to environments with high concentrations of metals (Diels et al., 2009). This is also found with extremely high concentrations of Mn(II), where a strain of *Ralstonia picketti* was able to survive and also remove the Mn(II) from aqueous solution possibly by biosorption onto hydroxyl and carbonyl groups on the bacterial surface, ultimately producing a precipitate (Huang et al., 2018). These bacteria also induce efficient efflux of copper transport using metallophores that can regulate uptake of metals into the cell instead of relying on passive transport that can be deadly (Kenney & Rosenzweig, 2018; von Rozycki & Nies, 2009). *Cupriavidus* is found colonizing metal abundant biotopes with their well-adapted metal resistance (Janssen et al., 2010). The biotopic relationship copper deposits have with these bacteria entwines their fates as they grow concurrently alongside each other.

The capability of surviving in oligotrophic environments coupled with high metal-resistance makes our reported genera particularly well-suited for Martian and Martian analogue environments. Two novel species of *Cupriavidus* were discovered in mudflow deposits from Mt. Pinatubo, where they exhibit chemolithoautotrophic growth using hydrogen, oxygen, and carbon dioxide in an area deprived of organic carbon (Sato et al., 2006). *Cupriavidus, Ralstonia,* and *Methylobacterium* were found on the Mars Odyssey Orbiter (prior to flight) and other space industry settings as described by Mijnendonckx et al. (2013). They described the metal resistance of *Cupriavidus metallidurans* and *Ralstonia picketti* using select metals as micronutrients. They found *Cupriavidus metallidurans* isolates to be able to withstand an excess of Cu^{2+} typically toxic to many species of bacteria. These bacteria's strong resistance to the antimicrobial disinfection and sterilization procedures of the space industry not only demonstrate their candidacy as extremophiles, but further their candidacy as potential contaminants that may be brought to Mars. The features of these bacteria that allow them to persist in difficult environments on Earth and potentially on Mars should also be considered when checking for contaminants in future missions.

4.3 Molecular biosignatures

Although the presence of colorful pigments in an environment deprived of light, such as lava tubes, could appear surprising, carotenoids and other pigments can play different roles depending on the metabolisms of the host cells. Carotenoid molecules have a wide distribution in very diverse organisms (more than 750 chemical structures determined to date), including extremophiles, where they serve several key functions at the cellular level. In addition to serving as photoprotective accessory pigments in phototrophic organisms, they have excellent antioxidant properties acting as reactive oxygen species (ROS) scavengers thus protecting

cellular DNA and proteins (Stahl & Sies, 2003). They are also believed to help stabilize membranes at low temperatures (Dieser et al., 2018), particularly relevant for Icelandic microbial communities. It has even been proposed that carotenoids played an important role in the early evolution of life on Earth (Alcaíno et al., 2016; Klassen, 2010) by being involved in membrane stabilization, prior to fatty acids (Ourisson & Nakatani, 1994). These functions and properties, essential for the highly UV-irradiated early Earth, might also be compatible with early Mars organisms (Cockell, 2002; Rothschild, 1990), adding to the relevance of carotenoids as a biosignature target for our search for life on Mars. In addition, although we would not normally expect phototrophic organisms in cave environments, cyanobacteria have recently been reported in deep subsurface rock samples on Earth, where they switch to a light-independent hydrogen-based lithoautotrophic metabolism (Puente-Sánchez et al., 2018).

Carotenoids may prove as a critical biosignature in our search for life in extraterrestrial lava tubes as they are only found in living organisms, are relatively easy to distinguish and detect, and have been shown to be highly resistant to oxidative and radiative stress in simulated Martian conditions (Baqué et al., 2016). Portable Raman instruments could potentially detect carotenoid molecules in caves*in situ* by humans or robotic explorers. As lava tubes are shielded from radiation on Mars, carotenoids have the potential to be preserved on even longer timescales. Potential pigmented species found in our DNA analysis of sample C2 occur in the genera *Cupriavidus*and *Methylobacterium.* These are thought to be the source of the carotenoids identified in the sample (Ramachandran et al., 2014; Osawa et al., 2015; Heider et al., 2012). The identification of carotenoids in our samples demonstrate a staying power in this copper-rich environment that may lend itself to future identification in caves as evidence of extant or extinct life.

5 Conclusion

The Planetary Analogues and Exobiology Lava Tube Expedition (PELE) was formed to investigate biosignatures in terrestrial lava tubes and inform the search for extant and extinct life in Martian lava tubes. Our*Study in Blue* , a case study of blue, copper-rich speleothems collected in Icelandic lava tubes, gave insights into how we might approach sampling these analogue environments, and what we might expect to find. A portable XRF gave us a good indication of elemental composition inside the caves and helped us distinguish regions of interest, i.e., secondary minerals with obvious variations in composition to that of the background lava rock. 16S rRNA sequencing of microbial mats revealed Proteobacteria as the dominant bacterial phylum, several carotenoid-containing genera, chemolithoautotrophic genera, and genera known for their high metal resistance, all characteristics which make them good candidates for surviving on Mars, but also potential contaminants in Mars missions. Raman analysis produced a prominent carotenoid signal, which is a promising biosignature feasibly detectable for robotic lava tube explorers carrying Raman instruments. The morphology and elemental composition of the blue secondary mineral precipitates were elucidated by SEM/EDS, identifying chrysocolla crusts, and a complex, layered precipitate consisting of chrysocolla, pseudomalachite, manganese (hydr)oxide, and a carbonate-bearing species. It appears that copper may be leached from hyaloclastite and ash deposits, enriching the rainwater and groundwater that filters into the caves. Copper-rich speleothems are then precipitated out and serve as biotopes for metal-resistant organisms. As chrysocolla and other oxidized copper mineral phases have been detected on the surface of Mars, they may also be present in Martian lava tubes, and if so, would be worthy targets for astrobiological investigations by future missions.

Acknowledgments

The Icelandic Speleological Society (ISS) was indispensable to this work, with in-depth knowledge of the terrain, and by doing their best to keep these caves in their pristine states by protecting them from human contamination by tourists or civilians, which is vital when collecting samples of microbial mats. Our guides Árni B. Stefánsson, Guni Gunnarsson, and Ingólfur Páll Matthíasson were delightful to work with, and we thank them with the utmost reverence for their professionalism and for sharing these subterranean natural wonders with our team.

Many thanks to Anett Blischke of the Icelandic GeoSurvey for constructing the geological map of Iceland in

Figure 1.

This work was supported by NWO ALWOP.274 and the University of Akureyri Research Fund (grant no. R1812).

M.B. acknowledges the support of the Deutsche Forschungsgemeinschaft (DFG – German Research Foundation) for the project "Raman Biosignatures for Astrobiology Research" (RaBioFAM; project number: 426601242) and of Geo.X, the Research Network for Geosciences in Berlin and Potsdam, for a travel grant.

B.R.S. is an inventor of patents and patent applications involving small molecule therapeutics, co-founded and serves as a consultant to Inzen Therapeutics and Nevrox Limited, and serves as a consultant to Weatherwax Biotechnologies Corporation and Akin Gump Strauss Hauer & Feld LLP.

Open Research

The data supplement to this work is accessible at https://public.yoda.uu.nl/geo/UU01/I32Z95.html, DOI: 10.24416/UU01-I32Z95. The geological map of Iceland was created using ArcGIS 10.8.1 and data at the Iceland GeoSurvey (Hjartarson & Sæmundsson, 2014), available at (*https://en.isor.is/geological-maps-geological-web-map*) and (*https://arcgisserver.isor.is/*). Figures were created with Prism software available at*https://www.graphpad.com/scientific-software/prism/*, and Krona (Ondov et al., 2011), available at*https://github.com/marbl/Krona/releases*. The raw DNA sequences were processed with the R package DADA2 (version 1.18.0) (Callahan, McMurdie, et al., 2016). DNA sequencing data was obtained using the Silva_132 database (Quast et al., 2013), available at *https://www.arb-silva.de/*, and the RDP naïve Bayesian classifier (Wang et al., 2007).

References

Alcaíno, J., Baeza, M., & Cifuentes, V. (2016). Carotenoid distribution in nature. *Carotenoids in Nature* , 3-33. https://doi.org/10.1007/978-3-319-39126-7_1

Anthony, J. W. (1990). *Handbook of mineralogy: Arsenates, phosphates, vanadates.* (Vol. 4). Mineral Data Pub.

Arnalds, O. (2010). *Dust sources and deposition of aeolian materials in Iceland* . https://skemman.is/handle/1946/19921

Arnalds, O. (2015). The Volcanic Aeolian Environments of Iceland. In *The Soils of Iceland* (pp. 139-152). Springer, Dordrecht. https://doi.org/10.1007/978-94-017-9621-7_11

Arnalds, O., Gisladottir, F. O., & Sigurjonsson, H. (2001). Sandy deserts of Iceland: an overview. *Journal of Arid Environments* ,*47* (3), 359–371. https://doi.org/10.1006/JARE.2000.0680

Baqué, M., Verseux, C., Böttger, U., Rabbow, E., de Vera, J. P. P., & Billi, D. (2016). Preservation of biomarkers from cyanobacteria mixed with Marslike regolith under simulated Martian atmosphere and UV flux.*Origins of Life and Evolution of Biospheres* , *46* (2–3), 289–310. https://doi.org/10.1007/s11084-015-9467-9

Baqué, M., Hanke, F., Böttger, U., Leya, T., Moeller, R., and Vera, J.-P. de (2018). Protection of cyanobacterial carotenoids' Raman signatures by Martian mineral analogues after high-dose gamma irradiation. *Journal of Raman Spectroscopy . 49* (10), 1617–1627. https://doi.org/10.1002/jrs.5449.

Berger, J. A., Schmidt, M. E., Gellert, R., Boyd, N. I., Desouza, E. D., Flemming, R. L., Izawa, M. R. M., Ming, D. W., Perrett, G. M., Rampe, E. B., Thompson, L. M., VanBommel, S. J. V., & Yen, A. S. (2017). Zinc and germanium in the sedimentary rocks of Gale Crater on Mars indicate hydrothermal enrichment followed by diagenetic fractionation.*Journal of Geophysical Research: Planets* , *122* (8), 1747–1772. https://doi.org/10.1002/2017JE005290

Blank, J. G., Agha-mohammadi, A. A., Bell Jr, E. R., Crown, D. A., Morrell, B., Patterson, C. J., ... & Whelley, P. L. (2021). Volcanic caves as priority sites for astrobiology science. *Bulletin of the American*

Astronomical Society , *53* (4), 306. https://doi.org/10.3847/25c2cfeb.1bc1e6cf

Boston, P. J., Spilde, M. N., Northup, D. E., Melim, L. A., Soroka, D. S., Kleina, L. G., Lavoie, K. H., Hose, L. D., Mallory, L. M., Dahm, C. N., Crossey, L. J., & Schelble, R. T. (2001). Cave biosignature suites: microbes, minerals, and mars. *Astrobiology* , *1* (1), 25–55. https://doi.org/10.1089/153110701750137413

Callahan, B. J., Mcmurdie, P. J., Rosen, M. J., Han, A. W., Johnson, A. J. A., & Holmes, S. P. (2016). DADA2: high-resolution sample inference from Illumina amplicon data. *Nature Methods* , *13* (7), 581-583. https://doi.org/10.1038/nMeth.3869

Callahan, B. J., McMurdie, P. J., Rosen, M. J., Han, A. W., Johnson, A. J. A., & Holmes, S. P. (2016). DADA2: High-resolution sample inference from Illumina amplicon data. *Nature Methods* , *13* (7). https://doi.org/10.1038/nmeth.3869

Candela, P. A., & Holland, H. D. (1984). The partitioning of copper and molybdenum between silicate melts and aqueous fluids. *Geochimica et Cosmochimica Acta* , *48* (2), 373–380. https://doi.org/10.1016/0016-7037(84)90257-6

Cockell, C. S. (2002). The Ultraviolet Radiation Environment of Earth and Mars: Past and Present. In G. Horneck & C. Baumstark-Khan (Eds.),*Astrobiology* . Springer Berlin Heidelberg. https://doi.org/10.1007/978-3-642-59381-9_15

Dickinson, W. H., Caccavo, F., & Lewandowski, Z. (1996). The ennoblement of stainless steel by manganic oxide biofouling.*Corrosion Science* , *38* (8), 1407–1422. https://doi.org/10.1016/0010-938X(96)00031-5

Diels, L., van Roy, S., Taghavi, S., & van Houdt, R. (2009). From industrial sites to environmental applications with *Cupriavidus metallidurans* . *Antonie Van Leeuwenhoek* , *96* (2), 247–258. https://doi.org/10.1007/s10482-009-9361-4

Dieser, M., Greenwood, M., Foreman, C. M., & Greenwood, M. (2018). Carotenoid pigmentation in antarctic heterotrophic bacteria as a strategy to withstand environmental stresses. *Arctic, Antarctic, and Alpine Research* , *42* (4), 396–405. https://doi.org/10.1657/1938-4246-42.4.396

Eason, D. E., & Sinton, J. M. (2009). Lava shields and fissure eruptions of the Western Volcanic Zone, Iceland: Evidence for magma chambers and crustal interaction. *Journal of Volcanology and Geothermal Research* , *186* (3–4), 331–348. https://doi.org/10.1016/J.JVOLGEORES.2009.06.009

Furnes, H. (1978). Element mobility during palagonitization of a subglacial hyaloclastite in Iceland. *Chemical Geology* ,*22* (C), 249–264. https://doi.org/10.1016/0009-2541(78)90034-7

Giachino, A., & Waldron, K. J. (2020). Copper tolerance in bacteria requires the activation of multiple accessory pathways. *Molecular Microbiology* , *114* (3), 377–390. https://doi.org/10.1111/MMI.14522

Gibson, I. L., Kirkpatrick, R. J., Emmerman, R., Schmincke, H. U., Pritchard, G., Oakley, P. J., Thorpe, R. S., & Marriner, G. F. (1982). The trace element composition of the lavas and dikes from a 3-km vertical section through the lava pile of eastern Iceland. *Journal of Geophysical Research* , *87* (B8), 6532–6546. https://doi.org/10.1029/JB087IB08P06532

Gounot, A. M. (1994). Microbial oxidation and reduction of manganese: Consequences in groundwater and applications. *FEMS Microbiology Reviews* , *14* (4), 339–349. https://doi.org/10.1111/j.1574-6976.1994.tb00108.x

Gunnarsdottir, M. J., Gardarsson, S. M., st. Jonsson, G., Armannsson, H., & Bartram, J. (2015). Natural background levels for chemicals in Icelandic aquifers. *Hydrology Research* , *46* (4), 647–660. https://doi.org/10.2166/nh.2014.123

Hannesdóttir, H., Zöhrer, A., Davids, H., Sigurgeirsdóttir, S. I., Skírnisdóttir, H., & Árnason, . (2010). Vatnajökull National Park: Geology and Geodynamics. *Northern Environmental Education Development. University of Iceland. Hornafjordur, Iceland: Hornafjordur Regional Research Centre* .

Haraldsson, K. Ö. (2001). *The Hekla 2000 eruption, distribution of ash from the first days of the eruption* (Doctoral dissertation, BSc Thesis, University of Iceland).

Hathaway, J. J. M., Garcia, M. G., Balasch, M. M., Spilde, M. N., Stone, F. D., Dapkevicius, M. D. L. N. E., Amorim, I. R., Gabriel, R., Borges, P. A. V., & Northup, D. E. (2014). Comparison of Bacterial Diversity in Azorean and Hawai'ian Lava Cave Microbial Mats. *Geomicrobiology Journal* , *31* (3), 205–220. https://doi.org/10.1080/01490451.2013.777491

Heider, S. A., Peters-Wendisch, P., & Wendisch, V. F. (2012). Carotenoid biosynthesis and overproduction in *Corynebacterium glutamicum* . *BMC microbiology* , 12(1), 1-11.

Hjartarson, A., & Sæmundsson, K. (2014). Geological map of Iceland, bedrock. 1: 600,000. *Iceland GeoSurvey, Reykjavík* .

Hoffmann, L. J., Breitbarth, E., Ardelan, M. v., Duggen, S., Olgun, N., Hassellöv, M., & Wängberg, S. Å. (2012). Influence of trace metal release from volcanic ash on growth of *Thalassiosira pseudonana*and *Emiliania huxleyi* . *Marine Chemistry* , *132–133* , 28–33. https://doi.org/10.1016/J.MARCHEM.2012.02.003

Huang, H., Zhao, Y., Xu, Z., Ding, Y., Zhang, W., & Wu, L. (2018). Biosorption characteristics of a highly Mn(II)-resistant Ralstonia pickettii strain isolated from Mn ore. *PLOS ONE* , *13* (8), e0203285. https://doi.org/10.1371/JOURNAL.PONE.0203285

Janssen, P. J., van Houdt, R., Moors, H., Monsieurs, P., Morin, N., Michaux, A., Benotmane, M. A., Leys, N., Vallaeys, T., Lapidus, A., Monchy, S., Médigue, C., Taghavi, S., McCorkle, S., Dunn, J., van der Lelie, D., & Mergeay, M. (2010). The complete genome sequence of*Cupriavidus metallidurans* Strain CH34, a master survivalist in harsh and anthropogenic environments. *PLOS ONE* , *5* (5), e10433. https://doi.org/10.1371/JOURNAL.PONE.0010433

Jones, M. T., & Gislason, S. R. (2008). Rapid releases of metal salts and nutrients following the deposition of volcanic ash into aqueous environments. *Geochimica et Cosmochimica Acta* , *72* (15), 3661–3680. https://doi.org/10.1016/J.GCA.2008.05.030

Kenney, G. E., & Rosenzweig, A. C. (2018). Chalkophores. *Annual Review of Biochemistry* , *87* , 645–676. https://doi.org/10.1146/ANNUREV-BIOCHEM-062917-012300

Kiernan, K., Wood, A. C., & Middleton, A. G. (2003). Aquifer structure and contamination risk in lava flows: insights from Iceland and Australia. *Environmental Geology* , *43* , 852–865. https://doi.org/10.1007/s00254-002-0707-8

Klassen, J. L. (2010). Phylogenetic and evolutionary patterns in microbial carotenoid biosynthesis are revealed by comparative genomics.*PLoS ONE* , *5* (6). https://doi.org/10.1371/journal.pone.0011257

Ladomersky, E., & Petris, M. J. (2015). Copper tolerance and virulence in bacteria. *Metallomics* , *7* (6), 957–964. https://doi.org/10.1039/C4MT00327F

Léveillé, R. J., & Datta, S. (2010). Lava tubes and basaltic caves as astrobiological targets on Earth and Mars: A review. *Planetary and Space Science* , *58* (4), 592–598. https://doi.org/10.1016/j.pss.2009.06.004

Little, B. J., & Wagner, P. A. (2018). Chapter 4. Spatial Relationships Between Bacteria and Mineral Surfaces. In J. F. N. K. H. Banfield (Ed.),*Geomicrobiology: Interactions between Microbes and Minerals* (pp. 123–160). De Gruyter. https://doi.org/10.1515/9781501509247-006

Mason, E., Wieser, P. E., Liu, E. J., Edmonds, M., Ilyinskaya, E., Whitty, R. C. W., Mather, T. A., Elias, T., Nadeau, P. A., Wilkes, T. C., McGonigle, A. J. S., Pering, T. D., Mims, F. M., Kern, C., Schneider, D. J., & Oppenheimer, C. (2021). Volatile metal emissions from volcanic degassing and lava–seawater interactions at Kīlauea Volcano, Hawai'i. *Communications Earth & Environment* ,*2* (1). https://doi.org/10.1038/s43247-021-00145-3

McMurdie, P. J., & Holmes, S. (2013). phyloseq: An R Package for Reproducible Interactive Analysis and Graphics of Microbiome Census Data. *PLOS ONE* , *8* (4), e61217. https://doi.org/10.1371/JOURNAL.PONE.0061217

Mergeay, M., van Houdt, R., Hobman, J., Monsieurs, P., & Vandenbussche, G. (2015). *Metal Response in Cupriavidus metallidurans Volume I: From Habitats to Genes and Proteins* (M. Mergeay & R. van Houdt, Eds.). Springer. https://doi.org/10.1007/978-3-319-20594-6

Mijnendonckx, K., Provoost, A., Ott, C. M., Venkateswaran, K., Mahillon, J., Leys, N., & van Houdt, R. (2013). characterization of the survival ability of *Cupriavidus metallidurans* and *Ralstonia pickettii* from space-related environments. *Microbial Ecology* ,*65* (2), 347–360. https://doi.org/10.1007/s00248-012-0139-2

Monchy, S., Benotmane, M. A., Janssen, P., Vallaeys, T., Taghavi, S., Van Der Lelie, D., & Mergeay, M. (2007). Plasmids pMOL28 and pMOL30 of*Cupriavidus metallidurans* are specialized in the maximal viable response to heavy metals. *Journal of bacteriology* ,*189* (20), 7417-7425.

Morosov, X., Davoudi, C. F., Baumgart, M., Brocker, M., & Bott, M. (2018). The copper-deprivation stimulon of *Corynebacterium glutamicum* comprises proteins for biogenesis of the actinobacterial cytochrome bc1-aa3 supercomplex. *Journal of Biological Chemistry* ,*293* (40), 15628–15640. https://doi.org/10.1074/jbc.RA118.004117

Nealson, K. H., Tebo, B. M., & Rosson, R. A. (1988). Occurrence and Mechanisms of Microbial Oxidation of Manganese. *Advances in Applied Microbiology* , *33* (C), 279–318. https://doi.org/10.1016/S0065-2164(08)70209-0

Northup, D. E., & Lavoie, K. H. (2001). Geomicrobiology of caves: A review. *Geomicrobiology Journal* , *18* (3), 199–222. https://doi.org/10.1080/01490450152467750

Northup, D. E., Melim, L. A., Spilde, M. N., Hathaway, J. J. M., Garcia, M. G., Moya, M., Stone, F. D., Boston, P. J., Dapkevicius, M. L. N. E., & Riquelme, C. (2011). Lava cave microbial communities within mats and secondary mineral deposits: implications for life detection on other planets. *Astrobiology* , *11* (7), 601–618. https://doi.org/10.1089/ast.2010.0562

Northup, D. E., Stefánsson, Á. B., Medina, M. J., Caimi, N. A., & Kooser, A. S. (2016). Microbial communities of Icelandic lava caves. In*Proc 16th Int Symp Vulcanospeleo* , *Ocean View, HI.*

Ondov, B. D., Bergman, N. H., & Phillippy, A. M. (2011). Interactive metagenomic visualization in a Web browser. *BMC Bioinformatics* ,*12* . https://doi.org/10.1186/1471-2105-12-385

Osawa, A., Kaseya, Y., Koue, N., Schrader, J., Knief, C., Vorholt, J. A., ... & Shindo, K. (2015). 4-[2-O-11Z-Octadecenoyl-β-glucopyranosyl]-4, 4'-diapolycopene-4, 4'-dioic acid and 4-[2-O-9Z-hexadecenoyl-β-glucopyranosyl]-4, 4'-diapolycopene-4, 4'-dioic acid: new C30-carotenoids produced by*Methylobacterium* . Tetrahedron Letters, 56(21), 2791-2794.

Ourisson, G., & Nakatani, Y. (1994). The terpenoid theory of the origin of cellular life: the evolution of terpenoids to cholesterol.*Chemistry & Biology* , *1* (1), 11–23. https://doi.org/10.1016/1074-5521(94)90036-1

Payré, V., Fabre, C., Sautter, V., Cousin, A., Mangold, N., Deit, L. le, Forni, O., Goetz, W., Wiens, R. C., Gasnault, O., Meslin, P. Y., Lasue, J., Rapin, W., Clark, B., Nachon, M., Lanza, N. L., & Maurice, S. (2019). Copper enrichments in the Kimberley formation in Gale crater, Mars: Evidence for a Cu deposit at the source. *Icarus* ,*321* , 736–751. https://doi.org/10.1016/j.icarus.2018.12.015

Popa, C., Carrozzo, F. G., Achille, D. G., Silvestro, S., Esposito, F., & Mennella, V. (2014). Evidences for copper bearing minerals in Shalbatana Valley, Mars. *45th Lunar and Planetary Science Conference* , 2340.

Puente-Sánchez, F., Arce-Rodríguez, A., Oggerin, M., García-Villadangos, M., Moreno-Paz, M., Blanco, Y., Rodríguez, N., Bird, L., Lincoln, S. A., Tornos, F., Prieto-Ballesteros, O., Freeman, K. H., Pieper, D. H., Timmis, K. N., Amils, R., & Parro, V. (2018). Viable cyanobacteria in the deep con-

tinental subsurface. *Proceedings of the National Academy of Sciences* , *115* (42), 10702–10707. https://doi.org/10.1073/PNAS.1808176115

Quast, C., Pruesse, E., Yilmaz, P., Gerken, J., Schweer, T., Yarza, P., Peplies, J., & Glöckner, F. O. (2013). The SILVA ribosomal RNA gene database project: improved data processing and web-based tools.*Nucleic Acids Research* , *41* (D1), D590–D596. https://doi.org/10.1093/NAR/GKS1219

Ramachandran, H., Iqbal, M. A., & Amirul, A. A. (2014). Identification and characterization of the yellow pigment synthesized by*Cupriavidus sp.* USMAHM13. *Applied biochemistry and biotechnology* , 174(2), 461-470.

Rose, W. I., Gu, Y., Watson, I. M., Yu, T., Bluth, G. J. S., Prata, A. J., Krueger, A. J., Krotkov, N. A., Carn, S., Fromm, M. D., Hunton, D. E., Ernst, G. G. J., Viggiano, A. A., Miller, T. M., Ballenthin, J. O., Reeves, J. M., Wilson, J. C., Anderson, B. E., & Flittner, E. (2003). The February-March 2000 eruption of Hekla, Iceland from a satellite perspective. *Geophysical Monograph Series* , *139* , 107–132. https://doi.org/10.1029/139GM07

Rothschild, L. J. (1990). Earth analogs for Martian life. Microbes in evaporites, a new model system for life on Mars. *Icarus* ,*88* (1), 246–260. https://doi.org/10.1016/0019-1035(90)90188-F

Rudnick, R. L., & Gao, S. (2003). Composition of the continental crust.*Treatise on Geochemistry* , *3–9* , 1–64. https://doi.org/10.1016/B0-08-043751-6/03016-4

Sanyal, S. K., Reith, F., & Shuster, J. (2020). A genomic perspective of metal-resistant bacteria from gold particles: Possible survival mechanisms during gold biogeochemical cycling. *FEMS Microbiology Ecology* , *96* (7), fiaa111.

Sato, Y., Nishihara, H., Yoshida, M., Watanabe, M., Rondal, J. D., Concepcion, R. N., & Ohta, H. (2006). *Cupriavidus pinatubonensis sp. nov.* and *Cupriavidus laharis sp. nov* ., novel hydrogen-oxidizing, facultatively chemolithotrophic bacteria isolated from volcanic mudflow deposits from Mt. Pinatubo in the Philippines.*International Journal of Systematic and Evolutionary Microbiology* , *56* , 973–978. https://doi.org/10.1099/ijs.0.63922-0

Sauro, F., Pozzobon, R., Massironi, M., de Berardinis, P., Santagata, T., & de Waele, J. (2020). Lava tubes on Earth, Moon and Mars: A review on their size and morphology revealed by comparative planetology. In*Earth-Science Reviews* (Vol. 209). Elsevier B.V. https://doi.org/10.1016/j.earscirev.2020.103288

Schmincke, H. U., Viereck, L. G., Griffin, B. J., & Pritchard, R. G. (1982). Volcaniclastic rocks of the Reydarfjördur drill hole, eastern Iceland: 1. Primary features. *Journal of Geophysical Research: Solid Earth* , *87* (B8), 6437-6458. https//doi.org/10.1029/JB087iB08p06437

Schock, M. R., Lytle, D. A., & Clement, J. A. (1995). Effect of pH, DIC, orthophosphate and sulfate on drinking water cuprosolvency. In*National Risk Management Research Lab Technical Report* . https://www.osti.gov/biblio/128476

Schulze-Makuch, D., & Irwin, L. N. (2004). *Life in the Universe* . Springer-Verlag.

Selensky, M. J., Masterson, A. L., Blank, J. G., Lee, S. C., & Osburn, M. R. (2021). Stable carbon isotope depletions in lipid biomarkers suggest subsurface carbon fixation in lava caves. *Journal of Geophysical Research: Biogeosciences* , *126* (7). https://doi.org/10.1029/2021JG006430

Sheth, H. (2018). Explosive Volcanism in Flood Basalt Provinces. *A Photographic Atlas of Flood Basalt Volcanism* , 171–194. https://doi.org/10.1007/978-3-319-67705-7_7

Smith, D. B., Zielinski, R. A., & Rose, W. I. (1982). Leachability of uranium and other elements from freshly erupted volcanic ash.*Journal of Volcanology and Geothermal Research* , *13* (1–2), 1–30. https://doi.org/10.1016/0377-0273(82)90017-8

Stahl, W., & Sies, H. (2003). Antioxidant activity of carotenoids.*Molecular Aspects of Medicine* , *24* (6), 345–351. https://doi.org/10.1016/S0098-2997(03)00030-X

Stivaletta, N., Barbieri, R., & Billi, D. (2012). Microbial colonization of the salt deposits in the driest place of the Atacama Desert (Chile). *Origins of Life and Evolution of Biospheres* ,*42* (2), 187–200. https://doi.org/10.1007/s11084-012-9289-y

Thordarson, T., & Self, S. (1993). The Laki (Skaftár Fires) and Grímsvötn eruptions in 1783–1785. *Bulletin of Volcanology* , *55* (4), 233-263.

Uckert, K., Chanover, N. J., Getty, S., Voelz, D. G., Brinckerhoff, W. B., Mcmillan, N., Xiao, X., Boston, P. J., Li, X., Mcadam, A., Glenar, D. A., & Chavez, A. (2017). The characterization of biosignatures in caves using an instrument suite. *Astrobiology* , *17* (12), 1203–1218. https://doi.org/10.1089/ast.2016.1568

Vítek, P., Osterrothová, K., & Jehlička, J. (2009). Beta-carotene—a possible biomarker in the Martian evaporitic environment: Raman micro-spectroscopic study. *Planetary and Space Science* , *57* (4), 454-459. https//doi.org/10.1016/j.pss.2008.06.001

von Rozycki, T., & Nies, D. H. (2009). Cupriavidus metallidurans: evolution of a metal-resistant bacterium. *Antonie van Leeuwenhoek* , *96* (2), 115–139. https://doi.org/10.1007/S10482-008-9284-5

Wang, Q., Garrity, G. M., Tiedje, J. M., & Cole, J. R. (2007). Naïve Bayesian classifier for rapid assignment of rRNA sequences into the new bacterial taxonomy. *Applied and Environmental Microbiology* ,*73* (16), 5261–5267. https://doi.org/10.1128/AEM.00062-07/

Yang, E., Sun, · Leni, Ding, · Xiaoyuan, Dongdong Sun, ·, Liu, J., & Wang, W. (2019). Complete genome sequence of *Caulobacter flavus*RHGG3 T, a type species of the genus Caulobacter with plant growth-promoting traits and heavy metal resistance. *3 Biotech* ,*9* (2), 42. https://doi.org/10.1007/s13205-019-1569-z

A Study in Blue: Secondary Copper-rich Minerals and Their Associated Bacterial Diversity in Icelandic Lava Tubes

Nina Kopacz[1], Joleen Csuka[2], Mickael Baqué[3], Iaroslav Iakubivskyi[4], Hrefna Guðlaugardóttir[5], Ingeborg J. Klarenberg[5,6], Mahid Ahmed[1], Alexandra Zetterlind[1], Abhijeet Singh[7], Inge Loes ten Kate[1], Eric Hellebrand[1], Brent R. Stockwell[2,8], Árni B. Stefánsson[9], Oddur Vilhelmsson[5,6,10], Anna Neubeck[7], Anna Schnürer[11], Wolf Geppert[12]

[1]Department of Earth Science, Utrecht University, the Netherlands, [2]Department of Chemistry, Columbia University, USA, [3]Institute of Planetary Research, German Aerospace Centre (DLR), Germany, [4]Tartu Observatory, University of Tartu, Estonia, [5]University of Akureyri, Iceland, [6]University of Iceland Biomedical Center, Iceland, [7]Department of Earth Sciences, Uppsala University, [8]Department of Biological Sciences, Columbia University, USA, [9]Augnlæknastofa ÁBS, Iceland, [10]University of Reading School of Biological Sciences, UK, [11]Swedish University of Agricultural Sciences, Sweden, [12]Stockholm University Astrobiology Centre, Sweden.

Corresponding authors: Nina Kopacz (k.a.kopacz@gmail.com), Joleen Csuka (joleen.csuka@gmail.com)

Key Points:

- Icelandic lava tubes are appropriate analogue test sites for multidisciplinary sampling protocols for future missions to Martian lava tubes
- Blue copper-rich speleothems serve as biotopes for metal-resistant organisms in lava tubes

Abstract

Lava tubes on Mars hold exciting potential for the preservation of biosignatures, which may survive on geological timescales in these isolated, stable environments. To support the development of future astrobiological mission concepts, we turn to terrestrial lava tubes, host to a variety of microbial communities and secondary minerals. Following a multidisciplinary sampling protocol, we retrieved biological, molecular, and mineralogical data from several lava tubes in Iceland. We report on blue-colored copper-rich secondary minerals and their associated bacterial communities using a multi-method approach, and an amalgam of 16S rRNA gene sequencing, Raman spectroscopy, scanning electron microscopy, and energy-dispersive X-ray spectroscopy data sets. We found numerous bacterial genera known for their high metal resistance and ability to survive in low-nutrient environments, both characteristics to be expected for any potential life in Martian lava tubes. Associated with them, we identified several types of copper-rich secondary minerals as well as carotenoid signals. If found in Martian lava tubes, blue copper-rich mineral precipitates would be deserving of astrobiological investigation, as they have potential to preserve biosignatures and harbor life.

1 Introduction

Cave environments on Earth have long provided shelter to a variety of organisms, from microbes to humans. Though their scales of interest differ vastly, these two examples have sought the same comfort from caves: a stable and sheltered environment, protected from the woes of the surface world. Since the discovery of lava caves on Mars (see (Sauro et al., 2020) for a review), they have become of renewed interest as targets for human shelter in future missions, as well as areas of astrobiological interest, with the potential of harboring traces of extant or extinct extraterrestrial life.

Recent years have seen a huge advancement in the development and miniaturization of autonomous mobility systems and exploration technologies for robotic missions to planetary caves, including instrument suites for *in situ* astrobiological studies (summarized in (Blank et al., 2020)). All aspects of cave mission preparation, from robotics development to astronaut training and scientific advancement, are currently being tested in terrestrial analogue sites, namely lava tubes in the Azores, Hawai'i, Iceland, Lanzarote, the western continental United States, and other volcanic areas.

Astrobiological studies in terrestrial lava tubes focus on the characterization of the microbe-mineral continuum and the identification of biosignatures in the form of biologically mediated speleothems (secondary cave minerals) and other geochemical fingerprints that may remain preserved on geological timescales (Boston et al., 2001; Léveillé & Datta, 2010; Northup et al., 2011; Northup & Lavoie, 2001). A suite of analyses is required to distinguish a biologically mediated secondary mineral from one that is abiotic (Uckert et al., 2017), presenting a difficult challenge**.** Nonetheless, a variety of biologically mediated speleothems has been reported in the literature, including filamentous manganese "snow", "crisco" moonmilk, lithified U-loops and living sulfuric acid "snotties", and pool fingers in limestone caves in New Mexico and Mexico (Boston et al., 2001).

Microbes in caves on Earth attach to minerals on cave walls, ceilings, or floors and initiate biomineralization reactions, creating biofilms. Biofilm formation is controlled by several processes, starting by initial microbe adhesion to the surface, governed by fluid flow and charging of the substratum. The initial colonizers excrete exopolysaccharides, which increase the surface irregularity and allow the biofilm to grow. Thus, the location of biofilm growth in caves depends not only on where particles and microbes can be transported to, but also be allowed to accumulate. A detailed review of the dynamics of biofilm formation on mineral surfaces and their spatial distribution is given by Little & Wagner (2018).

As the biofilm grows in layers away from the surface, it becomes a microbial mat of great complexity. Within its structure, chemical environments can exist that are radically different from that of the surrounding, allowing for the growth of minerals and microbes that would otherwise not be expected. Concentration of organic and inorganic particles can sustain a consortium of microorganisms of

different nutritional modes. The putatively high microbial diversity within the biofilm may create local changes in pH or redox conditions, which can facilitate the precipitation of minerals that are unstable outside of the biofilm. Microbes can control the precipitation of these minerals either passively, where microbial cells act as nucleation sites, or actively, where bacterially produced enzymes control mineralization (Northup & Lavoie, 2001).

The majority of life in the Universe is thought to be unicellular (Schulze-Makuch & Irwin, 2018). Moreover, the tendency to form biofilms and mats may well be an adaptation to be expected on other planets, with other biologies, and perhaps other fundamental chemistries (Boston et al., 2001). Regardless of their specific chemistries, metabolisms relying on differences in redox potentials in elements present in the lava rock can be expected for any initial colonizers in Martian lava caves, due to the absence of light and the oligotrophic (low nutrient) quality of caves on Mars. The chemolithoautotrophic nature of this hypothetical life may eventuate the production of similar speleothems as found in terrestrial caves. Basaltic terrestrial lava tubes are most similar in mineralogy to those posited on Mars and may thus provide analogous potential for chemolithoautotrophy, resulting in similar, recognizable molecular markers and biologically mediated speleothems.

To prepare a multidisciplinary sampling protocol for future astrobiological missions to caves on Mars, we set up the Planetary Analogues and Exobiology Lava Tube Expedition (PELE). Since 2017, we have explored lava fields and lava tubes on Hawai'i, the Azores, and Iceland. In this paper we focus on data from three lava tubes in two distinct regions of Iceland during a PELE field expedition in the summer of 2018, during which we collected samples of microbial mats and their geological substrates. We obtained *in situ* elemental data with a portable X-ray fluorescence (XRF) spectrometer, analyzed biological samples with 16S rRNA gene sequencing methods, biogeochemical samples with Raman spectroscopy, and geological samples with scanning electron microscopy (SEM) and energy-dispersive X-ray spectroscopy (EDS). In synergizing these data sets, we attempted to describe the biogeochemical fingerprints of microbial life in lava tubes and define their validity as biosignatures. While the microbial mats collected in the caves we visited came in a variety of colors, the blue samples are used here as a case study to exemplify our protocols, describe our workflow, and show the data that can be gleaned from such a study.

2 Materials and Methods

To gain a better understanding of what kinds of microbes thrive in oligotrophic, subterranean environments and the traces they leave behind, we analyzed an interdisciplinary set of samples collected in Icelandic lava tubes. Lava tubes are isolated, fragile, and potentially dangerous environments, and as such their exploration requires much care, planning, and specialized equipment.

2.1 Icelandic lava tubes

During a field expedition in the summer of 2018, we explored four lava tubes

in two distinct regions of Iceland: the southern Eldhraun lava field and the northern Ódáðahraun lava field. The caves, marked with black stars on Figure 1, are labeled B and C in the Eldhraun lava field (basaltic, intermediate, and acidic lavas since 1100 AD), and H and R in the Ódáðahraun lava field (basaltic, intermediate, and acidic lava flows older than 1100 AD). The moss-covered Eldhraun lava field is part of the Laki lava flow originating from the Laki (Skaftfir Fires) fissure eruption in southern Iceland near the older Mt. Laki hyaloclastite formation during 1783 and 1784. The eruption produced 14.7 ± 1.0 km^3 of basaltic lava flow, with 2.6% of the erupted volume in the form of tephra and ash (Thordarson & Self, 1993). The Ódáðahraun lava field is a sandy lava desert 5 000 km^2 in size, composed of many older lava flows sometimes covered by recent pumice deposits (Sheth, 2018). The oldest lava flow originated 10-12 thousand years ago, and the youngest lava flow is from the Holuhraun eruption in 2014-2015 (Hannesdóttir et al., 2010). Within this huge expanse sits Mt. Herðubreið, a classic table mountain, with hyaloclastite formations under its lava cap. Countless lava tubes abound in the Eldhraun and Ódáðahraun lava fields, many of which have been explored by the Icelandic Speleological Society (ISS), who have noted and archived their locations, and worked extensively to keep them pristine and protected from human contamination.

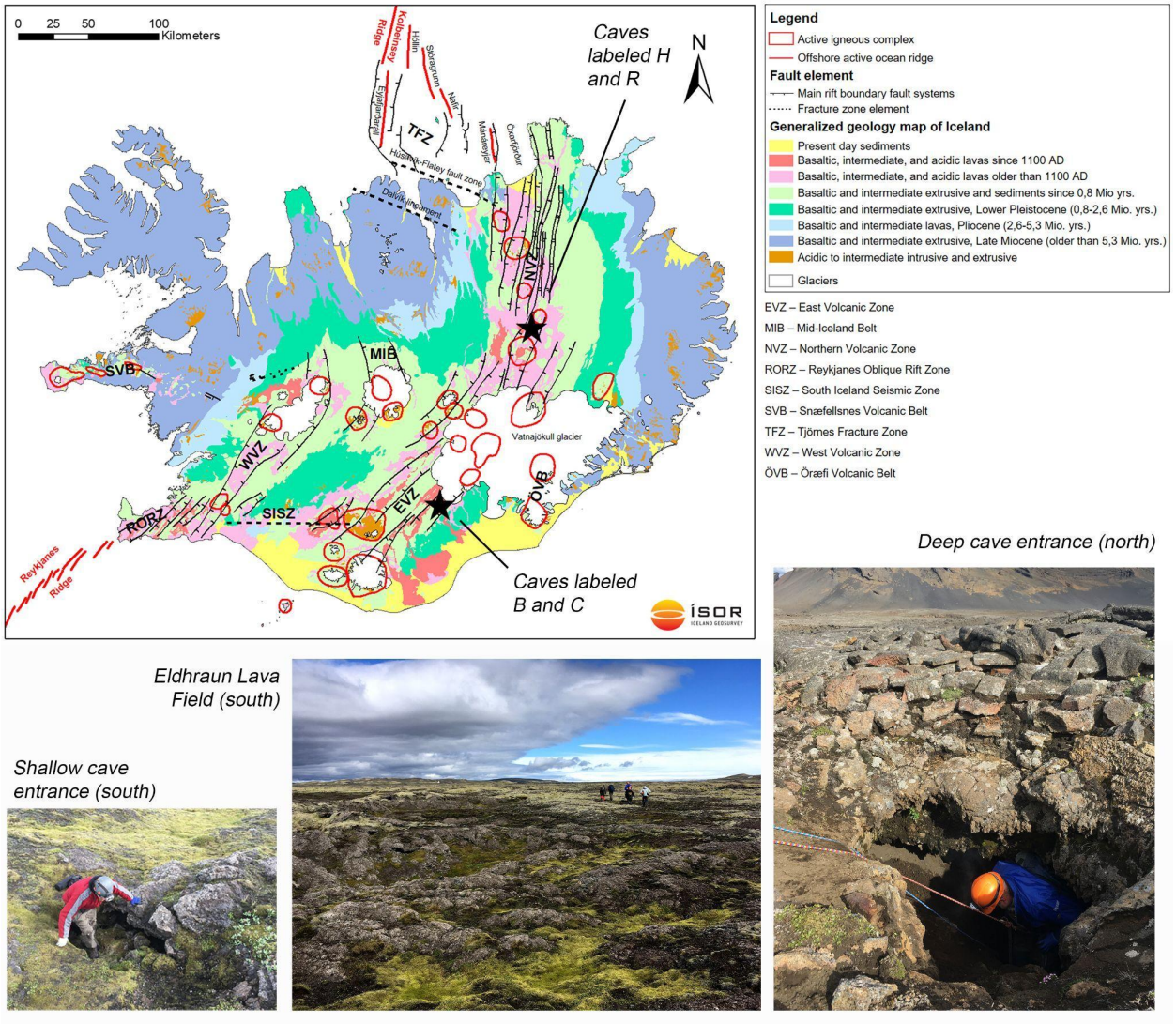

Figure 1. (top) Geological map of Iceland with black stars marking approximate cave locations. Map projection is ISN93. Courtesy of Anett Blischke, Icelandic GeoSurvey. **(bottom)** Lava fields visited and examples of cave entrances.

The Icelandic caves play host to a variety of microbial communities, as seen by microbial mats scattered across the cave ceilings, walls, and floors in all colors of the rainbow. Although the lava tubes themselves originate from relatively young flows (Figure 1), they also show some secondary mineral alteration. What is microbial mat and what is secondary mineral can often be difficult to distinguish, as their textures and colors can be interchangeable to the naked eye, and is

compounded by the knowledge that they may be intricately linked.

Blue-colored mats/mineral precipitates observed in Icelandic lava tubes were often found on surfaces of flowing water or along cracks in cave walls or ceilings, where water seeps in from the ground above (Figure 2). Some blue features had a viscous texture (Figure 2b), while others were brittle mineral crusts attached to the lava rock beneath (Figure 2a). The blue features found in caves B, C, and H (Figure 4) are the subject of this paper, as well as a detailed account of their acquisition in an effort to inform the search for biosignatures in future missions to lava caves on Mars.

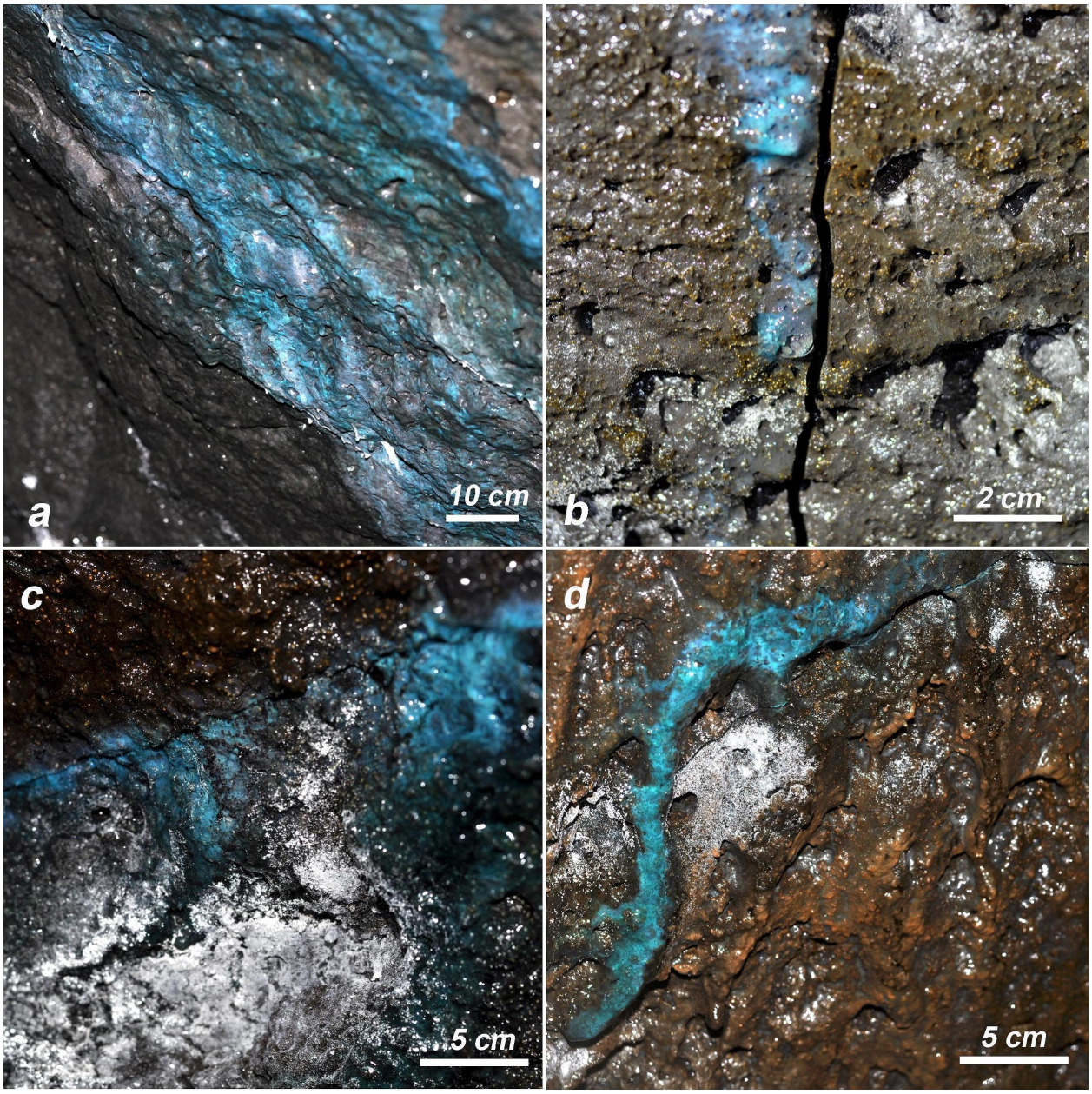

Figure 2. Examples of blue features. Blue mats and mineral precipitates are often found on surfaces of flowing water **(a)**, or along cracks in cave walls or ceiling, where water seeps in from the ground above **(b-d)**.

2.2 Sampling strategy

Sampling sites were kept minimal in size, with great care taken to touch as

little of the cave walls as possible, so as not to disturb or contaminate the microbial mats, which have a slow growth rate due to the environmental conditions and nutrient availability, taking several decades to reach macroscopic size. Speleothems, which form on geological timescales, are frequently vandalized, for example, the breaking of stalactites and stalagmites for personal collections and home decoration. Though sometimes unavoidable when sampling, such as when bumping the ceiling or walls in tight spaces, great care was taken to minimize damage of the mineral formations.

Initial training by cave connoisseur Diana Northup at a summer school in 2016 in the Azores organized by the European Astrobiology Campus, followed by several expeditions with the same core team honed the following 5-step sampling strategy (see also Figure 3).

Step 1. Trace gas analysis, performed by one person to measure CO_2, SO_2, NH_3, H_2S and NO_x, which have the potential to be dangerously high in caves.

Step 2. Microbial mat sampling, by scraping the mat off the rock under sterile conditions for DNA extraction and 16S rRNA gene sequencing analysis.

Step 3. Biogeochemical sampling, by chipping away a section of mat-covered rock with a geological hammer under sterile conditions for molecular analysis.

Step 4. Recording of the elemental composition of the rock below the scraped mats using a handheld XRF spectrometer.

Step 5. Geological sampling by chipping away the surface rock with a geological hammer for mineralogical analysis.

Figure 3. Sampling strategy. **(a)** Cave entrance to cave H, 12 m below ground. **(b)** Sampling in pairs: one sampler and one assistant handling cleaning and handing over of tools. **(c)** Biological sampling (step 2): scraping mats from the cave wall. **(d)** Handheld XRF measurements of cave wall (step 4). **(e)** Substrate sampling with a geological hammer and Falcon tube (steps 3 and 5).

2.2.1 Biomass sampling for DNA analysis

In order to minimize contamination, the second step in the sampling technique (after step one: ensuring the team's safety with the trace gas analyzer) was the collection of biomass for DNA extraction and sequencing (Figure 3c). Sampling began by sterilizing sample tools, i.e. scoops and spatulas with cleaning acetone and 70% ethanol, eliminating potential organic contaminants. We wore nitrile gloves washed with 70% ethanol, and used scoops and sterile Eppendorf tubes to scrape the surface of the lava tube to collect the overlying biomass. The sampling was best done with two people, one doing the sampling and one assisting with cleaning and in handing over tools and sampling tubes (Figure 3b). Samples were collected in biological triplicate to ensure enough samples for any repeated analyses. Samples were then stored at 4°C onsite and for shipment and finally at -20°C until the DNA extraction protocol began.

2.2.2. Biogeochemical sampling for molecular analysis

The third step in sampling was the collection of geological samples covered in biomass. We sterilized tools using the same acetone and 70% ethanol-based sterilization technique as for DNA sampling and used sterile 50 mL Falcon tubes to catch the biomass-covered rock samples that we chipped off with the hammer, which was flame sterilized with a lighter in addition to the solvent cleaning (Figure 3e). Collected in triplicate, these samples were also stored at 4°C to ensure minimal alteration of biomolecules.

2.2.3 Portable X-ray Fluorescence (XRF)

A portable NitonTM XL3t GOLDD+ X-Ray Fluorescence Analyzer from Thermo Fischer gave us elemental data *in situ* (step 4). It can detect up to 30 elements from Mg to Bi in the standard range without helium or vacuum assistance. The measured concentration of the sample must be at least three times the standard deviation of the measurement (i.e., detection limit); the measurement confidence is 95% (two sigma). "Mining mode" (best for analyzing raw or semi-processed mineral samples of varying density) was used for elemental quantification. The instrument was placed against the cave wall, measuring both the biofilm substrate post biological sampling as well as nearby uncolonized locations with an analysis time of 90 seconds.

2.2.4 Geological sampling of the lava tube substrate

Geological sampling was the fifth and final step in the sampling protocol. We chipped off rock samples from the cave wall with a geological hammer and stored them in ziplock bags under ambient conditions. The samples were then analyzed with SEM/EDS.

2.3 Characterization of microbial samples

To obtain phylogenetic data we performed DNA extractions, PCR amplification, and genetic sequencing on the microbial samples collected in step 2 of the sampling procedure.

2.3.1 DNA extractions

Genomic DNA was extracted in triplicate from the biofilm samples using a method previously used with environmental rock samples with phototrophic communities (Stivaletta et al., 2012). First a washing step was performed, wherein 200 µL (or weight equivalent ~200 mg) of the samples were resuspended in 1.5 mL of TE pH 8 (10 mM Tris Hydrochloride pH7.4 + 1mM EDTA pH 8), centrifuged at 10000 rpm for 10 min, after which the supernatant was discarded, and the pellets resuspended in 400 µL of TE pH 8. Then, the solution was added to sterile tubes with glass beads (Lysing Matrix tubes, MP Biomedicals, 1.4 mm ceramic beads, 0.1 mm silica spheres and one 0.4 mm glass sphere) and subjected to a bead beater two times 60 s at 6 m/s (MP Biomedicals, FastPrep24). Subsequently, 300 µL of phenol saturated with 0.1 M Tris Hydrochloride (tris-phenol, pH 7.4) and 300 µL of chloroform/isoamyl alcohol (24:1) were added to the tubes, and subjected to three 2-min cycles of heating at 60°C and vortexing for 30 s. After centrifugation (10 000 rpm, 5 min) the aqueous phase was extracted once with tris–phenol/chloroform/isoamyl alcohol (25:24:1); then 1/5 volume of TE buffer was added, and the pellet extracted again with phenol. Finally, the aqueous phases were extracted with chloroform/isoamyl alcohol (24:1) and nucleic acids precipitated overnight at -20°C with cold absolute ethanol and 0.3 M sodium acetate. After centrifugation (10 000 rpm, 5 min) and washing with 1 mL cold (-20°C) 75% ethanol, the pellets were dried out and resuspended in 30 µL nuclease free water.

2.3.2 PCR Amplification, Library Preparation and Sequencing

PCR amplification was made with PuRe Taq Ready-To-Go PCR Beads (GE Healthcare), 1 µL of each Illumina barcoded forward and reverse primers (16S rRNA gene V4 region primers 515F: GTGBCAGCMGCCGCGGTAA and 805R: GACTACHVGGGTATCTAATCC), 2 µL of DNA template, and 21 µL of nuclease-free water. The PCR cycling program used was 98°C for 30 s (denaturation), 35 cycles of 10 s at 98°C, 30 s at 60°C, 4s at 72°C, and 2 min at 72°C.

The multiplexed amplicon library was prepared by pooling equal amounts (20 ng) of each sample and paired-end sequencing was performed (at the SNP&SEQ Technology Platform, SciLife Labs, Sweden) on Illumina MiSeq with 300 base pairs (bp) read length using v3 sequencing chemistry. Raw sequences were processed with the R package DADA2 (version 1.18.0) (Callahan, Mcmurdie, et al., 2016). Due to low quality reverse reads affecting the merging of paired ends, we only used forward reads in the downstream analysis. Reads were truncated to 220 bp and assigned taxonomy using the Silva_132 database (Quast et al., 2013) and the RDP naïve Bayesian classifier (Wang et al., 2007). ASVs (Amplicon Sequence Variants) were normalized by Cumulative Sum Scaling. All samples with less than 100 reads were excluded from the analysis,

and biological triplicate samples were merged. Visualization was done using the R packages phyloseq (v1.34.0) (McMurdie & Holmes, 2013) and ggplot2 (Wickham, 2016), and Krona plots were made with Krona (Ondov et al., 2011).

2.4 Characterization of geochemical and geological samples

To characterize the geological substrate and identify any molecular biomarkers therein, we analyzed the geochemical samples collected in step 3 using confocal Raman microscopy and the geological samples collected in step 5 using SEM/EDS. The geochemical samples were first pulverized with a mortar and pestle under sterile conditions. The geological samples were polished into thin sections without any prior treatment and coated with platinum or carbon (when carbon content was not analyzed).

2.4.1 Confocal Raman microscopy

Raman spectra were obtained with a confocal WITec alpha 300 system, at the DLR Berlin, consisting of a microscope equipped with a 10x long working distance objective with a 0.25 numerical aperture, a piezo-driven scan table, a UHTS 300 spectrometer with an ultrafast EMCCD detector and a frequency-doubled Nd:YAG laser. The excitation wavelength of the laser was 532 nm, the spot diameter at the sample was ~2.5 µm and the spectral resolution of the spectrometer was 4-5 cm^{-1}. Integration time and laser power were varied according to the investigated sample (1-10 s and 0.1-7 mW respectively) to produce spectra with a sufficient signal-to-noise ratio, and to prevent sample damage/degradation and detector saturation.

2.4.2 SEM/EDS analysis of thin sections

Secondary electron (SE) and backscattered electron (BSE) images of platinum and carbon-coated thin sections were obtained using a Zeiss GeminiSEM 450 Field Emission Gun Scanning Electron Microscope at Utrecht University, using 10-20 keV accelerating voltage, a 250-1000 pA probe current, and a 10 mm working distance. The SEM was coupled with a windowless Oxford Instruments Ultim-Extreme EDS detector to characterize the elemental composition of the minerals present in the thin sections. Overview element distribution maps (15-60 min counting time) and point ID measurements (30 s counting time) were acquired at voltage of 20 keV and 1 nA, using Oxford Instruments Aztec software v5.1. For improved spatial chemical resolution in finely zoned domains, an accelerating voltage of 10 keV was used, acquiring the L-alpha intensity of Cu.

3 Results

To investigate cave biosignatures, we carried out fieldwork in Icelandic lava tubes, where we collected biological, biogeochemical, and geological samples, and *in situ* elemental data using a multi-step sampling protocol. We then characterized the samples using a variety of

analytical techniques. Here we describe the results in sections based on the location of the collected samples, the type of sample, and the analytical technique used.

3.1 Surface & subsurface field observations

3.1.1 Sampling sites

The caves sampled include caves B and C in the southern Eldhraun lava field, and H and R in the northern Ódáðahraun lava field (Figure 1). The lava rock in the caves visited appears largely unaltered, and the presence of microbial mats is much scarcer than that seen by our team and others (Hathaway et al., 2014) in lava tubes in the Azores. Still, we observed alteration minerals and microbial mats of various, striking colors.

The cave entrances in the southern Eldhraun lava field are very shallow, and the entirety of the tubes is no more than two meters below the surface. The temperature was measured at 8°C, and much water condensation was observed on the cave walls, of which we measured a pH of 8.1 near the sampling sites. In cave B we observed white, red, yellow, and blue mats on top of the cave walls, while in cave C we found green, blue, red, and white mats.

The cave entrance to cave H in the Ódáðahraun lava field was twelve meters below the surface, requiring four connected three-meter-long ladders, and additional propelling equipment for the team as a fail-safe. The entrance of cave R was equally deep, but accessible by foot down a steep ash mound. Compared to the southern caves, the temperature in the northern caves was colder, measured at 3°C, the cave ceilings were higher, and the walls generally appeared much drier. We observed many blue and purple mats, orange and yellow mats, grey slime, black dots, and fluffy white deposits on the cave walls. While most microbial mats seemed to be randomly dispersed on the cave walls, the blue precipitates occurred only where water was present, such as along cracks in the cave walls (Figure 3).

3.1.2 Samples collected

A variety of mat colors were sampled, including white, yellow, orange, grey, purple, and blue. The blue mats were distinct from the others in their incredible vibrancy of color, and in their consistent occurrence in places of flowing water, near cracks in the cave wall or ceiling, or in puddles on the ground. Blue mat and rock samples were collected in caves B, C, and H (Figure 4). Blue features were found surrounding a crack in cave B (Figure 4a), on a water droplet on a ceiling in cave C (4b), and at two sample sites in cave H, one on the wall (4c) and one in a puddle on the ground (4d). While the puddle in Figure 4d was very wet, offering up a wealth of viscous material for biological sampling, not all of the sampling locations were so generous. The blue material on the cave wall in Figure 4c was fused to the rock and had to be scraped off with much

patience.

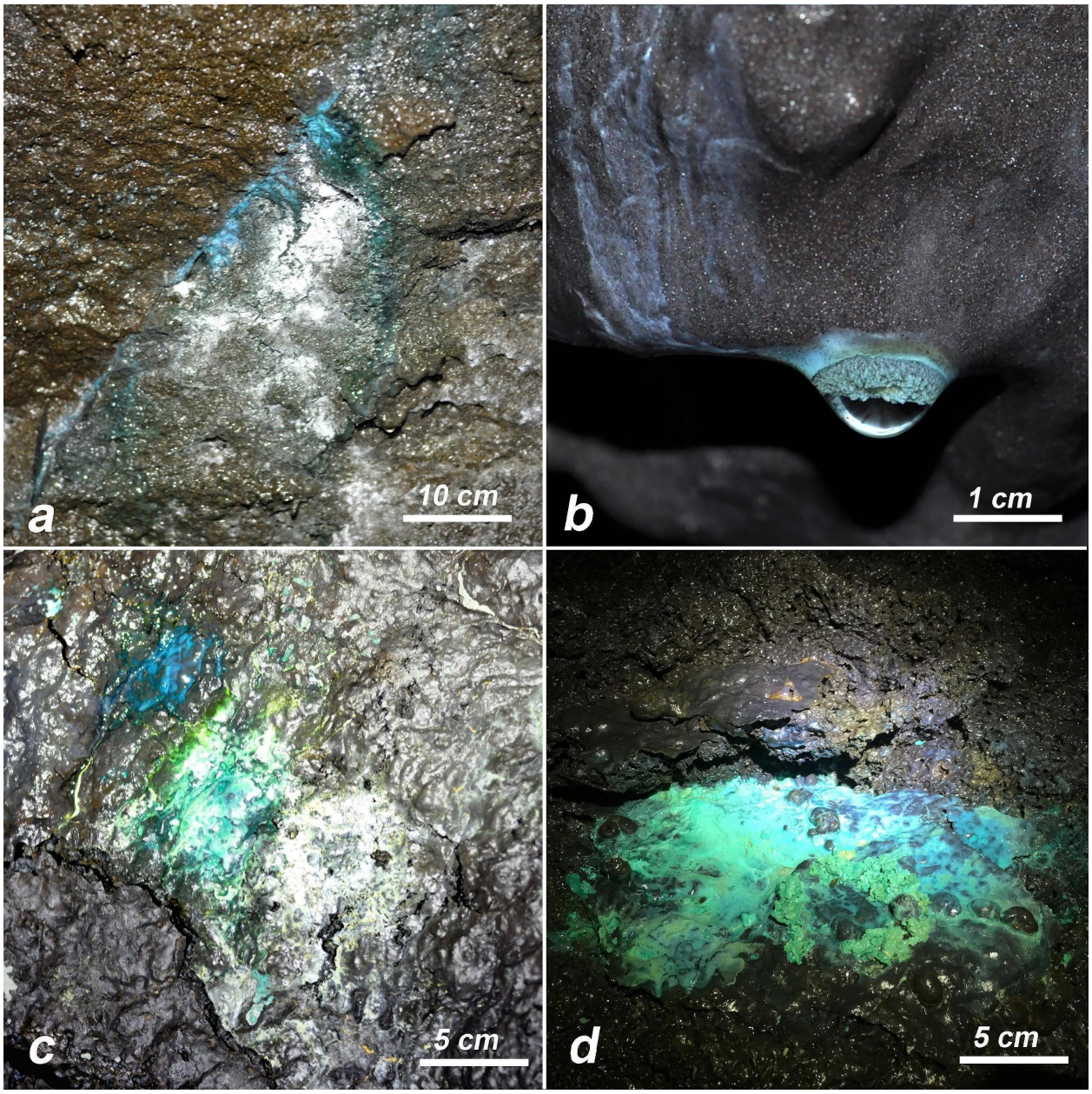

Figure 4. Sampling sites of blue features. **(a)** Sample B5 from cave B. **(b)** Sample C2 from cave C. **(c)** Sample H1 from cave H. **(d)** Sample H7 from cave H.

3.2 Blue Sample Analysis

Blue features were found to have prominent copper enrichments with our portable XRF while sampling them. We thus grouped these into one study and analyzed them further with 16S rRNA gene sequencing methods, Raman spectroscopy, and SEM/EDS in an attempt to understand the cause for such high concentrations of copper in an environment where it is expected to be scarce. The analyses performed on each sample can be seen in Table 1.

Cave Name	Sample	Analyses Performed	Relevant Figures
B (south)	B5	SEM/EDS	4a, 9
C (south)	C2	XRF, 16S rRNA sequencing, Raman	4b, 5c, 6a-f, 8
H (north)	H1	XRF	4c, 5a-c
H (north)	H7	XRF, 16s rRNA sequencing, SEM/EDS	4d, 5c, 6a-d, 7, 10

Table 1. Overview of blue samples and analyses performed.

3.2.1 X-Ray Fluorescence

XRF analysis of sample H1 (Table 1) of the mat substrate versus the background (collected from a region close to the sampling spot not covered by mat) revealed several differences between the elements present. Iron, calcium, silicon, magnesium, titanium, and manganese were decreased in mat substrate samples as compared to the background, while copper, phosphorus, and aluminum were lower in the background and higher in the mat-covered samples (Figure 5a). The mat substrate samples showed a striking enrichment in copper, which given the amount of aluminum and silicon present, could be in the form of a hydrated copper silicate. The Al:Cu:Si ratio of the mat substrate versus the background is shown in Figure 5b.

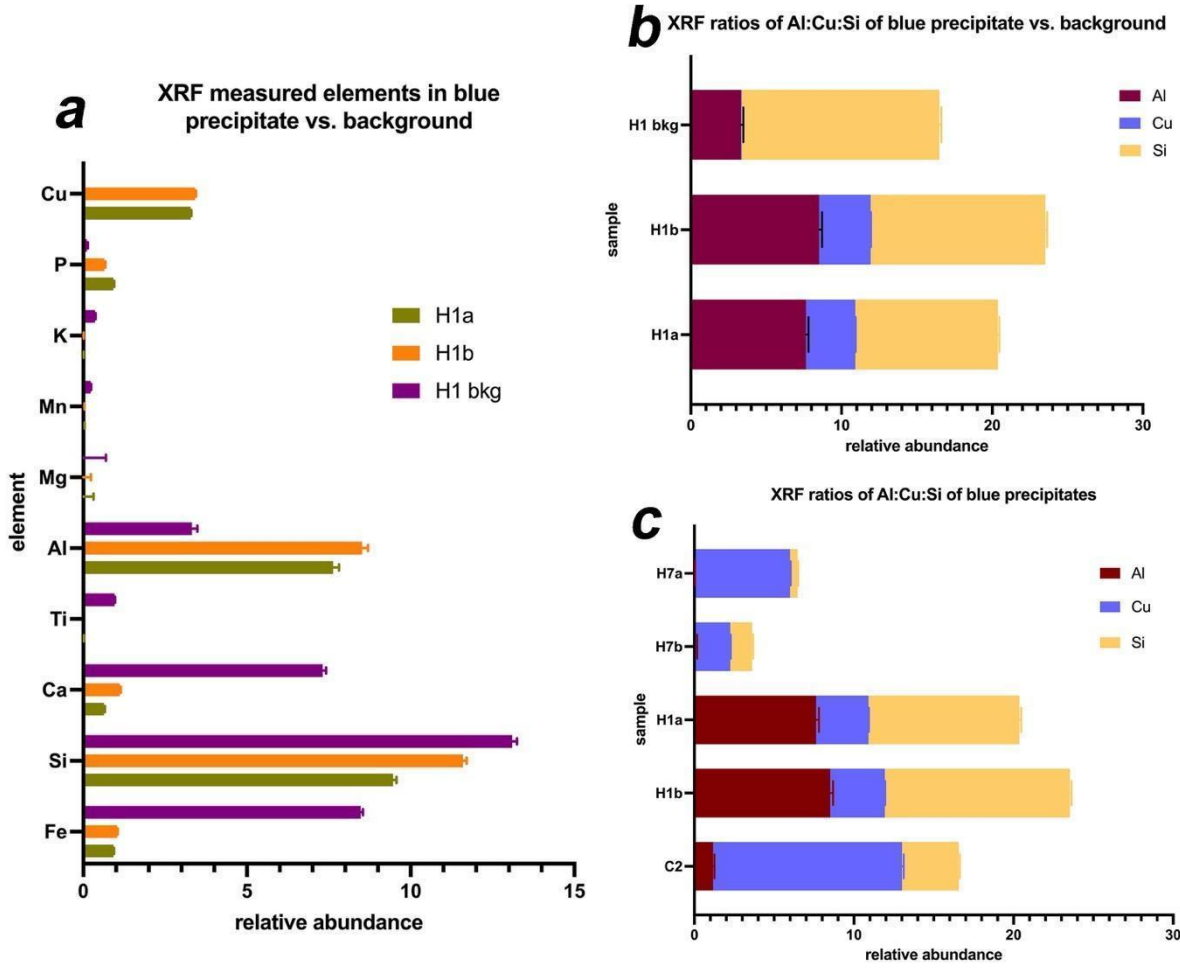

Figure 5. XRF measurements of blue precipitates in sample H1 vs. background. **(a)** Major elements were measured by pointing the XRF onto the cave wall where the mat was collected, vs. the background, i.e., a spot on the wall nearby not covered in mat. **(b)** Ratios of select elements aluminum, copper, and silicon in blue precipitate vs. background. Copper is markedly absent in the background. **(c)** Al:Cu:Si ratios measured in all blue precipitates.

Figure 5c shows the Al:Cu:Si ratio of samples C2 (0.33:3.3:1), H1a (0.81:0.35:1), H1b (0.73:0.29:1), H7a (0:12.8:1) and H7b (0.07:1.6:1). A typical Al:Cu:Si ratio of chrysocolla, an amorphous, hydrated copper silicate, is 0.12:1.98:1 (Anthony, 1990), and is in the same range as samples C2 and H7b.

3.2.2 DNA sequencing

Blue samples C2 (from cave C in southern Iceland) and H7 (from cave H in northern Iceland) were analyzed for bacterial community composition based on DNA extracted using phenol/chloroform with ethanol precipitation and amplified using V4-specific 16S rRNA gene primers (Figure 6). At the phylum level (Figure 6a, b), Proteobacteria strongly dominated the bacterial community composition. The most common family was Burkholderiaceae in both samples (Figure 6a, b). C2 and H7 contained a number of similar genera (Figure 6c), notably *Ralstonia* (Proteobacteria) *(*74% in C2 and 74% in H7) and *Caulobacter* (Proteobacteria) (20% in C2 and 5% in H7). The genera *Corynebacterium* (Actinobacteria), *Cutibacterium* (Actinobacteria), and *H1* (Bacteroidetes) were only found in sample C2, while *Cupriavidus* (Proteobacteria), *Methylobacterium-Methylorubrum* (Proteobacteria), and *Thermovirga* (Synergistaceae) were found exclusively in sample H7. No archaeal 16S rRNA sequences were detected.

3.2.3 Confocal Raman Spectroscopy

Sample C2 in Cave C was analyzed using confocal Raman spectroscopy. A drop of water hanging from the ceiling containing a significant amount of blue precipitate was observed under the microscope and identified with brown speckles incorporated in the crystalline deposit (Figure 6d). The Raman spectrum of the brown speckle shows prominent peaks at 1008, 1155, and 1513 cm^{-1}, typical of a carotenoid signature (Figure 6e). The 1008 cm^{-1} peak corresponds to the in-plane rocking modes of the CH_3 groups attached to the polyene chain, while the peak at 1155 cm^{-1} is associated with C-C stretching and C-H deformation, and the one at 1516 cm^{-1} with C=C stretching (Vítek et al., 2009; Baqué et al., 2018).

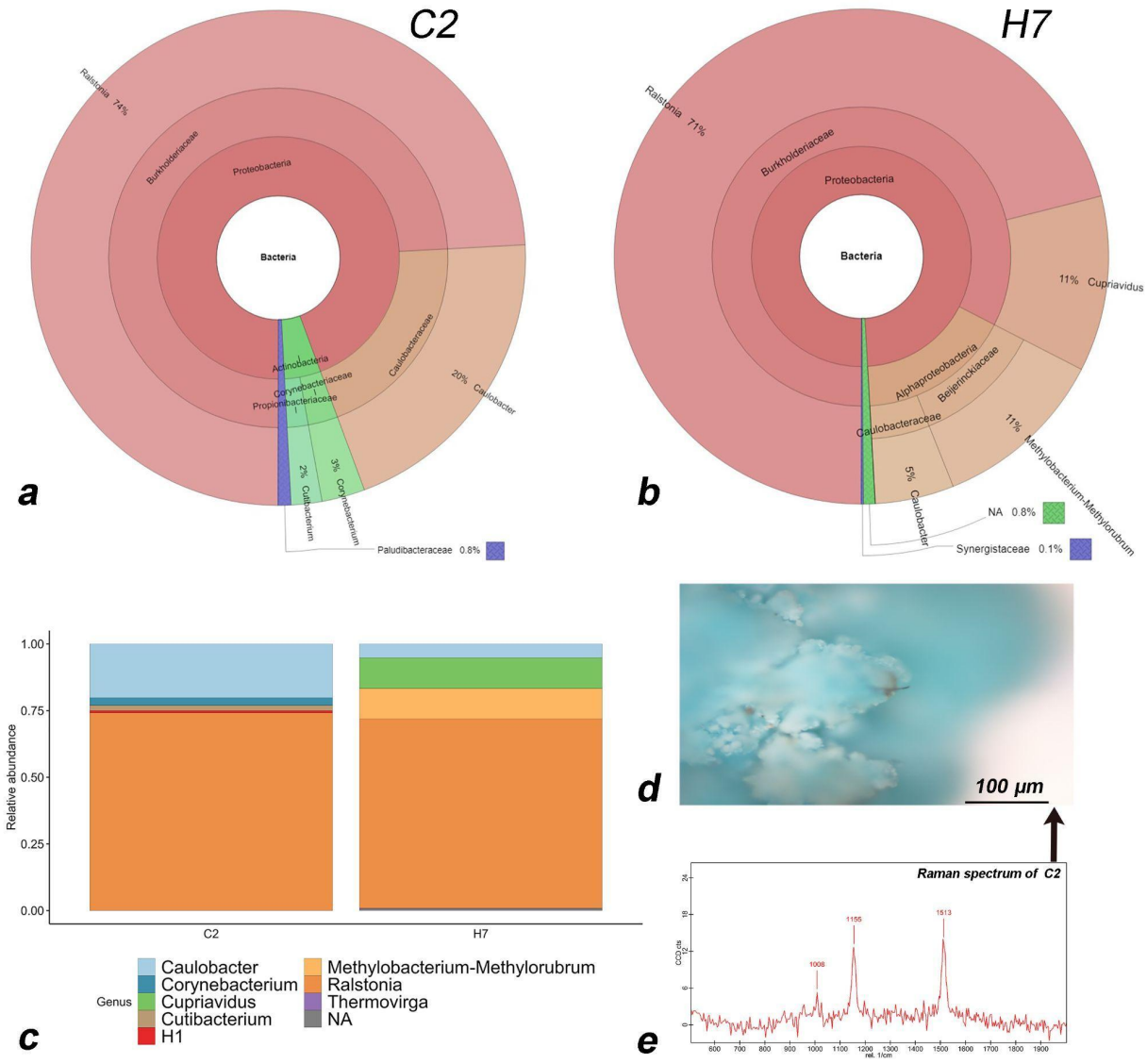

Figure 6. DNA sequencing and Raman spectroscopy results. **(a)** Krona plot of C2 showing relative abundances of Phyla, Classes, Orders, Families and Genera. **(b)** Krona plot of H7. **(c)** Bar plot showing relative abundance of genera of C2 and H7. **(d)** Optical microscopy image of blue drop material (sample C2) with visible brown speckles. **(e)** Raman spectrum of brown speckle inside blue drop material, with prominent peaks at 1008, 1155, and 1513 cm^{-1} typical of a carotenoid signature.

3.2.4 SEM/EDS analysis of thin sections

Figure 7 shows a comprehensive summary of the igneous minerals of the lava rock in the sample H7 thin section. The lava rock is composed of unaltered basalt, as seen from the pristine and angular grain boundaries. The igneous mineralogy consists mainly of clinopyroxene, ilmenite, and plagioclase. Igneous titano-magnetite has exsolved into Ti-poor magnetite and ilmenite. Phosphorus enrichment in tiny crystals in interstitial melt pockets suggests apatite saturation, in agreement with a highly evolved residual melt composition left after high degrees of crystallization.

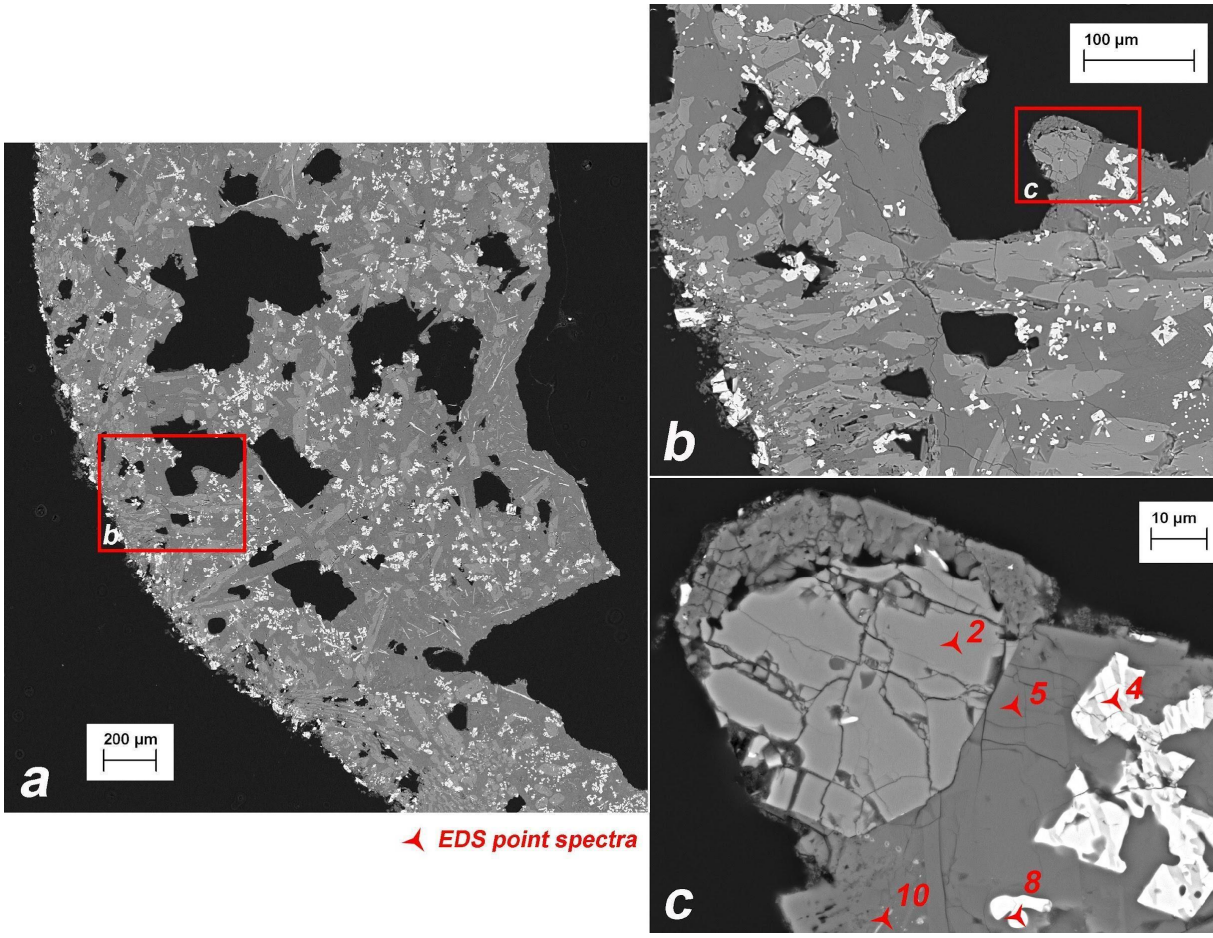

Figure 7. Igneous mineralogy. **(a-c)** Backscattered electron (BSE) images of sample H7 thin section, showing clear, angular grains indicating largely unaltered basalt. **(c)** EDS point spectra taken of spots marked in red, revealing typical basaltic mineralogy: augitic clinopyroxene (2), dendritic titano-magnetite, (oxy-) exsolved into a fine intergrowth of Ti-poor magnetite (white) and ilmenite

(slightly less bright) (4), plagioclase (5), magnetite (8), and apatite growth, indicating a highly evolved interstitial melt pocket (10). The spectra can be seen in Supporting Information.

Upon closer inspection of the thin section edges, surfaces potentially exposed to microbial mats, we see a ~10 m thick secondary mineral crust with a botryoidal, layered appearance in sample C2 (Figure 8a, b). It shows many fractures and damage, and is only sporadically present, suggesting it is fragile and not well-preserved in the sample handling and thin section preparation process. It also appears to have been deposited on top of the igneous rock, rather than leached from it, based on the clear boundary between the two and the independent growth pattern of the precipitate.

Another location in sample C2 with the secondary mineral crust was found and mapped with EDS (Figure 8c). The EDS spectrum in Figure 8i shows an augitic clinopyroxene as an igneous phase of the parent lava rock, which forms a sharp, unaltered boundary to the Ca-free crust (Figure 8e). The EDS spectrum of the crust (Figure 8h) shows a prominent copper enrichment, along with aluminum and silicon, and minor sulfur. The element maps shown in Figures 8f and 8g indicate that the copper enrichment in the crust is associated with uniformly high aluminum intensities. In addition, the crust material was observed to form shrinkage cracks under high vacuum and exposure to the (low-current) electron beam, consistent with a hydrous mineralogy. This resembles the signature of the hydrated copper silicate chrysocolla (Anthony, 1990), supported by the botryoidal, blue appearance. The crust has uniform, percent-level phosphorus concentrations.

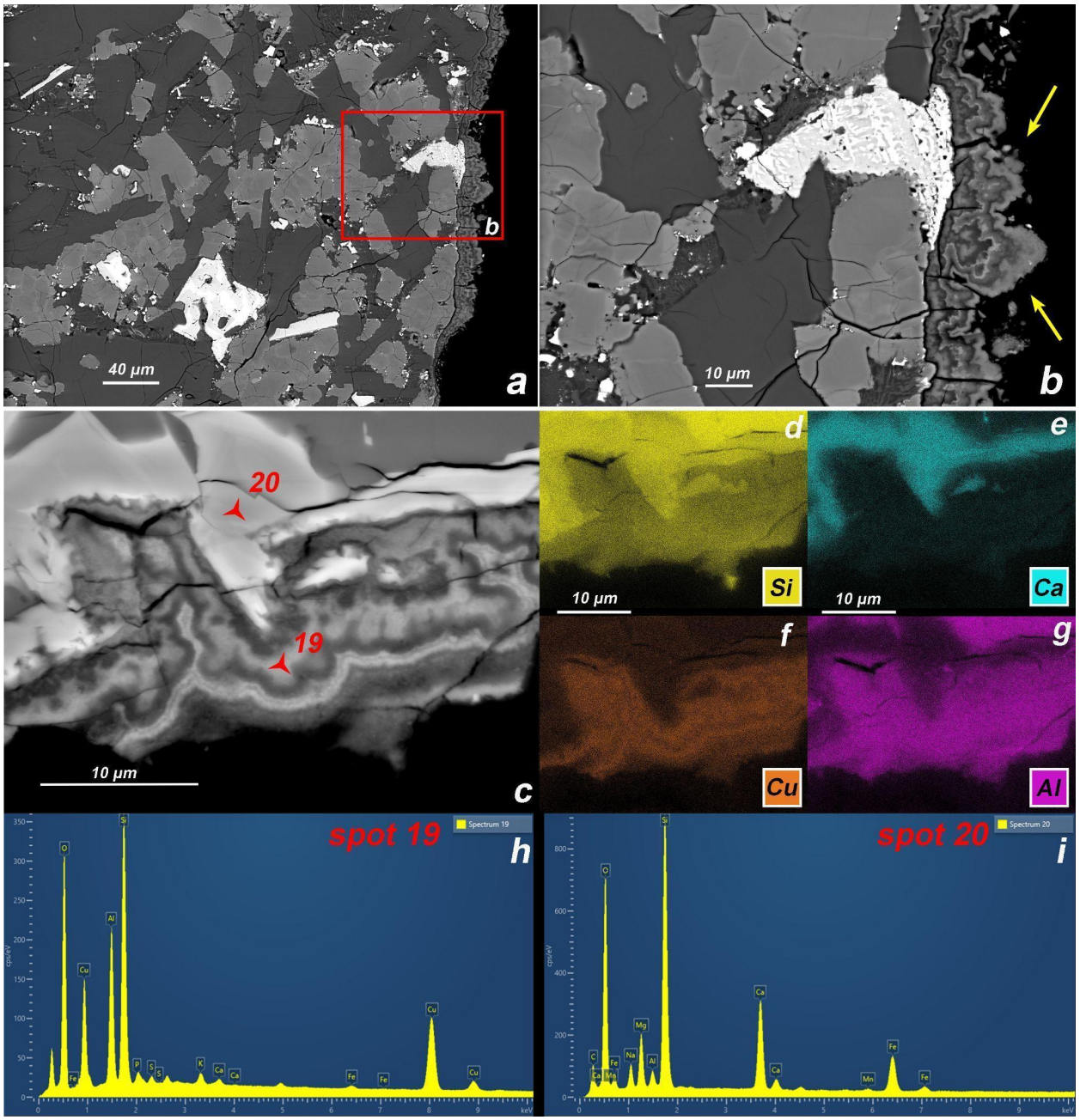

Figure 8. Botryoidal secondary mineral precipitate. **(a)** BSE image of a botryoidal, layered secondary mineral crust deposited on the edge of the igneous rock in sample C2. **(b)** Zoom-in on botryoidal crust, indicated by the yellow arrows. **(c)** BSE image of the botryoidal mineral crust in another location in C2.

(d-g) Elemental maps of silicon, calcium, copper, and aluminum present in the section presented in (c). **(h)** EDS spectrum of spot 19 (secondary mineral, pane c), showing copper and aluminum enrichment, possibly indicative of chrysocolla. **(i)** EDS spectrum of spot 20 (lava rock, pane c), showing unaltered augitic pyroxene.

In sample B5 from Cave B, we observed a more complex secondary mineral precipitate, with additional elemental enrichments and more discrete layering (Figure 9). This precipitate was not as botryoidal in appearance as that of sample C2, but was also enriched in copper and displayed distinct layering when mapped with EDS. It is clear that the copper occurs in the entirety of the deposit alongside all other elements (Figure 9f), however the amount of aluminum it is associated with varies in the different layers (Figure 9g). Additionally, there is a manganese-enriched layer that occurs in a silicon- and aluminum-poor region, as seen when comparing Figures 9e to 9d and 9g.

We were able to better distinguish the distribution of elements in the precipitate by mapping a small area with an excitation voltage of 10 keV for better spatial resolution of elements (Figure 9h). The EDS map sum spectrum in Figure 9m shows copper, aluminum, manganese, and phosphorus enrichments. The elemental maps confirm that manganese occurs in silicon-poor regions (Figure 9i) and that manganese and aluminum are competing (Figure 9j). Comparing Figure 9j to 9i and 9k, it is evident phosphorus enrichment occurs in silicon-poor regions, suggesting discrete phosphate minerals that contain copper. The outer layer of the complex crust is carbonate-bearing, as seen by the increased carbon level in the elemental map in Figure 9l, distinctly separate from the strong carbon signal produced by the epoxy above it.

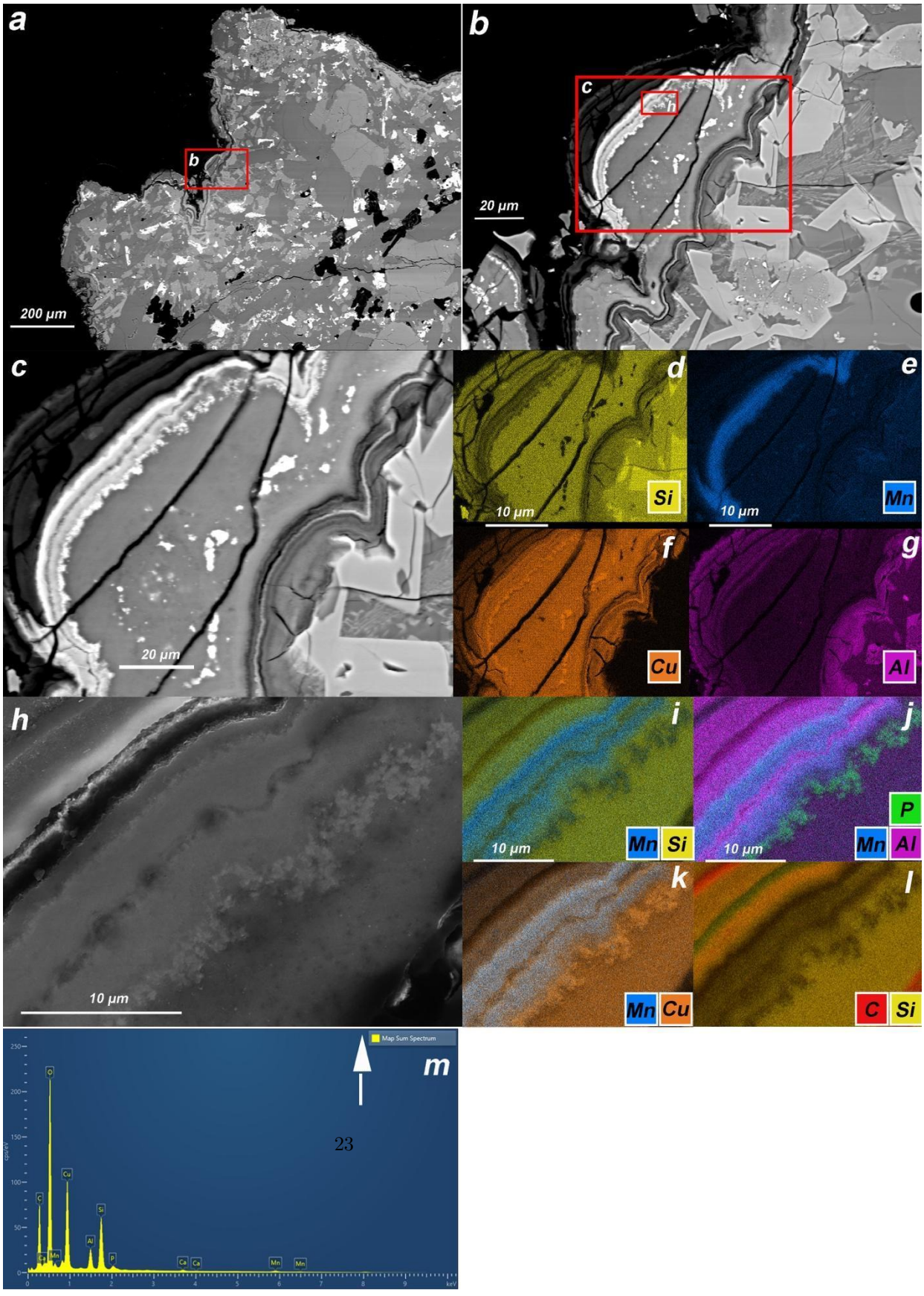
a
b
200 µm
b
c
h
20 µm
c
20 µm
d
Si
10 µm
e
Mn
10 µm
f
Cu
g
Al
h
10 µm
i
Mn Si
10 µm
j
P
Mn Al
10 µm
k
Mn Cu
l
C Si
m
Map Sum Spectrum
O
C
Cu
Si
Al
P
Ca Ca
Mn Mn
keV

Figure 9. Complex secondary mineral precipitate. **(a-c)** BSE image of a secondary mineral crust deposited on the edge of the igneous rock in sample B5 thin section. **(d-g)** Elemental maps of silicon, manganese, copper, and aluminum. **(h)** BSE image of close-up of secondary mineral crust. **(i-l)** Composite elemental maps of manganese and silicon **(i)**, phosphorus, manganese, and aluminum **(j)**, manganese and copper **(k)**, and carbon and silicon **(l)**. **(m)** EDS sum spectrum of (h) showing copper, phosphorus, and manganese enrichment. The EDS sum spectrum of (c) can be seen in Supporting Information.

These elemental maps suggest that a variety of minerals are precipitating alongside each other in the complex secondary mineral precipitate in Figure 9c, starting with an aluminum-poor copper silicate on the bottom right, followed by a copper phosphate, a manganese oxide or hydroxide, an aluminum-rich copper silicate, and topped off with a carbonate-bearing layer. The aluminum-rich copper silicate may be chrysocolla as discussed in previous sections. Pseudomalachite could be a candidate for the copper phosphate species based on the elemental distribution, and that it is similar in outward appearance and known to be associated with chrysocolla.

4 Discussion

We first gave a thorough description of our workflow in the field, explaining how we approach subterranean Martian analogue environments in search for biosignatures. We then presented a case study of blue microbial mats and their substrates from three lava tubes in Iceland analyzed with a variety of analytical techniques, namely a portable XRF, 16S rRNA gene sequencing, Raman spectroscopy, and SEM/EDS. Here we discuss the possible origins of the copper-rich secondary mineral precipitates, the significance of the bacteria that inhabit them, and the molecular markers they leave behind therein.

4.1 Cave geology and speleothems

We observed stark differences in elemental concentration (with preliminary *in situ* XRF readings) between the substrates where the microbial mats were sampled and the background areas, i.e., uncolonized areas nearby the sampling locations (Figure 5a-c). This demonstrates an altered geological substrate that biofilms either contribute to or benefit from in order to thrive in this environment.

Our mineralogical and elemental analysis of the lava rock substrate (Figure 7) and blue secondary mineral precipitates (Figures 8-10) show sequestering of elements more generally dispersed and scarce in basaltic lava tubes, particularly copper. The boundaries between the unaltered basalt and the precipitate rim, as seen in the SEM images of the thin sections (Figures 8 & 9), are pristine, dictating that the elements that make up the observed blue mineral precipitates must

have filtered in with the water through cracks in the cave walls or ceiling, instead of being leached from the host rock.

4.1.1 Sources of copper in Iceland

The average copper content of recent Icelandic basaltic lava is low, in the range of 10-200 ppm (g/g) (Eason & Sinton, 2009; Gibson et al., 1982), with occasional higher values found in older Miocene volcaniclastic rocks (Schmincke et al., 1982). Similarly, the copper content of Icelandic groundwater is also low, ranging from 0.00015 to 0.00209 ppm (Gunnarsdottir et al., 2015) where the Cu(II) ion is the more common oxidation state (Schock et al., 1995). However, copper is a semi-volatile element that can partition into a volatile-rich fluid that can physically separate from magma (Candela & Holland, 1984). Copper has been observed to be enriched in volcanic laze plumes from basaltic intraplate volcanoes, which can transfer it directly into the marine biosphere (Mason et al., 2021), and result in highly copper-enriched groundwater in specific areas. In the case of Iceland, copper is enriched in hyaloclastite deposits at the lava-ice interface (Furnes, 1978) and from there could be readily mobilized into groundwater that can infiltrate the lava tubes through cracks. In addition, rain and melting snow could be leaching copper from the volcanic ash that abounds on the lava fields above, bringing it into the tubes through cracks and cave openings. Kiernan et al. (2003) has noted the hydrogeological significance of lava tubes in the Eldhraun lava field, with rainwater and floods transporting glacio-aeolian deposits in these efficient groundwater flow channels.

Volcanic ash, derived from explosive eruptions of evolved intermediate-silicic volcanoes, has an evolved nature relative to basaltic lava flows, characterized by an enrichment in many incompatible elements, including copper. Hoffmann et al. (2012) showed that copper was released from various volcanic ash samples in concentrations up to 0.00065 ppm after just 15 min of contact with seawater. Smith et al. (1982) reported an average concentration of 0.39 ppm of Cu in leachates from volcanic ash in experiments simulating its interaction with rainfall and prolonged exposure with groundwater. Experiments with volcanic ash from the 2000 eruption of the Mt. Hekla volcano in Iceland showed a Cu flux of 0.069 ppm within 8 hours of mixing with deionized water (Jones & Gislason, 2008). Though this eruption would not have reached our areas of interest at the initial deposition stage, the volcanic cloud spewed out 0.1 Tg of ash (Rose et al., 2003), allowing it to be transported north-northeast by wind and depositing up to 5 kg/m^2 on the headwaters of the Ytri–Rangá River (Haraldsson, 2001).

There could thus exist many sources of copper in the Ódáðahraun and Eldhraun lava fields, including the hyaloclastite formations in nearby Mt. Laki and Mt. Herðubreið. The precise source of ash in the Ódáðahraun lava field is difficult to determine, as wind plays a large role in transportation of ash and sand, and a large proportion of it (some of which may be copper-rich ash and shattered hyaloclastite material) has been blown long distances over the lavas from sources closer to Vatnajökull glacier or the Jökulsá á Fjöllum glacial river (Arnalds, 2015). Indeed both the Ódáðahraun and Eldhraun lava fields are subject

to severe wind erosion and very high aeolian deposition rates (Arnalds, 2010; Arnalds et al., 2001), constantly replenishing the areas with volcanic ash.

4.1.2 Copper abundance on Mars

The surface of Mars is enriched in sulfur (Rudnick & Gao, 2003), and is thus expected to show elevated concentrations of chalcophile elements such as copper in the crust (Payré et al., 2019). Copper abundance values up to 580 ppm were detected by the Curiosity rover in the Liga sedimentary bedrock at Gale Crater (Berger et al., 2017). A chrysocolla bearing unit, along with pseudomalachite and other copper mineral phases, has been identified in the Shalbatana Valley palaeolacustrine system on Mars, and is hypothesized to be a supergene alteration product of copper sulfide minerals interacting with oxygen and water (Popa et al., 2014). This indicates a redox system capable of oxidizing Cu^{+} to Cu^{2+} in an oxidizing environment in Mars' past, which would likely have extended to lava tubes. Copper enrichments seemingly precipitated from groundwater have been found adsorbed to manganese deposits in the Kimberley Formation in Gale Crater on Mars, and are thought to be deposited in oxidizing conditions within fractures in the bedrock (Payré et al., 2019).

4.1.2 Blue speleothems in Iceland

In Figures 8-10 we described copper-rich secondary mineral precipitates as elucidated by SEM/EDS. While Figure 8 and 10 show a single copper phase, Figure 9 boasts a more complex precipitate, with discrete layers of copper silicates, copper phosphates, manganese oxides, and carbonate-bearing species. The copper phases present are expected to be mostly in the Cu(II) oxidation state, as this is the ion more readily available in the groundwater (Schock et al., 1995), and because of the prominent blue color (Cu(I) minerals are generally red/brown).

Chrysocolla, an amorphous copper phyllosilicate, was found in samples C2 (Figure 8), B5 (Figure 9), and H7 (Figure 10). A similar finding was previously reported in lava tubes in Kipuka Kanohina Cave Preserve in Hawai'i by Northup et al. (2011), who also found a blue drop filled with a precipitate with an Al:Cu:Si ratio of 0.15:1.8:1 as analyzed by EDS, comparable to a typical chrysocolla ratio of 0.12:1.96:1 (Anthony, 1990). We also identified a layer of pseudomalachite in sample B5, which has been hinted at often being associated with microbial mats (Little & Wagner, 2018).

Manganese oxides can be deposited by microbes in waters with manganese concentration as low as 10-20 ppb (Dickinson et al., 1996). Manganese oxidation is associated with the metabolism of several genera of bacteria. *Leptothrix* (a Proteobacteria associated with strictly low concentrations of organic matter) has been shown to deposit amorphous MnO_2 (vernadite) and a black MnO_2 precipitate (birnessite) (Gounot, 1994), while *Bacillus* has been observed to re-

crystallize birnessite to octahedral Mn_3O_4 (hausmannite) (Nealson et al., 1988). Boston et al. (2001) found manganese oxides in limestone caves to be linked to biogenic activity, identifying biogenically precipitated manganese 'snow' in limestone caves using a suite of analyses, including culturing Mn-oxidizing bacteria isolated from the 'snow' and observing them produce amorphous manganese oxides in the laboratory.

Ultimately, blue, copper-rich speleothems are attractive targets for astrobiological research, as they house bacterial communities resistant to elevated copper content. Should they occur in lava tubes on Mars, they could also be thought of as a biotope within the caves, host to extremophilic organisms.

4.2 Bacterial communities inhabiting blue mineral precipitates

The bacteria found in copper-enriched areas in the caves are present there because they can tolerate such an environment, and they actively sequester and adsorb copper ions. The significance of the bacteria identified and their copper-coping mechanisms are discussed below.

Proteobacteria was the major phylum identified in the blue samples in the southern cave (C2) and northern cave (H7). Families and genera were generally similar across the samples, with some notable deviations. Differences in environment (average cave temperature, age of lava tube, humidity, etc.) may contribute to the differences in bacteria present inside of the caves from north to south; however, there was a large overlap in the major abundances found. A recent study (Selensky et al., 2021) suggests that surface environment is not a major factor in organic nutrient cycling in lava tubes, which further exemplifies them as isolated environments that may harbor chemolithoautotrophic organisms and biosignatures that are useful in the search for life in extraterrestrial lava tubes. Furthermore, Northup et al. (2016) found that bacterial diversity in Icelandic lava tubes differed substantially from that in surface soil samples, with the most abundant cave phylum being Actinobacteria, followed by Acidobacteria and Proteobacteria.

The majority of genera detected in the blue samples (C2 and H7) represent copper-resistant oligotrophs. *Ralstonia, Caulobacter, Cupriavidus,* and *Corynebacterium* accounted for 97% of the relative genus abundance in sample C2 (Figure 6a). In sample H7 *Ralstonia, Cupriavidus, Caulobacter,* and *Methylobacterium-Methylorubrum* accounted for a total of 99% of the relative abundance (Figure 6b). *Ralstonia, Caulobacter, Cupriavidus*, and *Corynebacterium* are reported to have high metal resistance, which explains their presence in high copper concentration regions of the caves (Janssen et al., 2010; Mergeay et al., 2015; Morosov et al., 2018; Yang et al., 2019). Copper

is essential for bacteria in trace amounts as it is utilized as a micronutrient as well as an enzymatic cofactor for redox activities (Giachino & Waldron, 2020). Copper resistance is found in different mechanisms within the bacteria, the most ubiquitous being a) oxidation of Cu(I) to Cu(II), a less toxic ion to bacteria; b) copper sequestration by metallothioneins and c) transmembrane copper export (Ladomersky & Petris, 2015). Additionally, the genome of *Cupriavidus metallidurans* contains *cop* genes, which are highly induced by Cu(II) and encode for copper exporting P1B-type ATPases (Monchy et al., 2020), and *cueO* genes encoding for multicopper oxidase (Sanyal et al., 2020).

Much of the literature discusses the ability of both *Cupriavidus* and *Ralstonia* to adsorb metals to their cell membrane. Morphological changes can be seen as they adjust to environments with high concentrations of metals (Diels et al., 2009). This is also found with extremely high concentrations of Mn(II), where a strain of *Ralstonia picketti* was able to survive and also remove the Mn(II) from aqueous solution possibly by biosorption onto hydroxyl and carbonyl groups on the bacterial surface, ultimately producing a precipitate (Huang et al., 2018). These bacteria also induce efficient efflux of copper transport using metallophores that can regulate uptake of metals into the cell instead of relying on passive transport that can be deadly (Kenney & Rosenzweig, 2018; von Rozycki & Nies, 2009). *Cupriavidus* is found colonizing metal abundant biotopes with their well-adapted metal resistance (Janssen et al., 2010). The biotopic relationship copper deposits have with these bacteria entwines their fates as they grow concurrently alongside each other.

The capability of surviving in oligotrophic environments coupled with high metal-resistance makes our reported genera particularly well-suited for Martian and Martian analogue environments. Two novel species of *Cupriavidus* were discovered in mudflow deposits from Mt. Pinatubo, where they exhibit chemolithoautotrophic growth using hydrogen, oxygen, and carbon dioxide in an area deprived of organic carbon (Sato et al., 2006). *Cupriavidus, Ralstonia,* and *Methylobacterium* were found on the Mars Odyssey Orbiter (prior to flight) and other space industry settings as described by Mijnendonckx et al. (2013). They described the metal resistance of *Cupriavidus metallidurans* and *Ralstonia picketti* using select metals as micronutrients. They found *Cupriavidus metallidurans* isolates to be able to withstand an excess of Cu^{2+} typically toxic to many species of bacteria. These bacteria's strong resistance to the antimicrobial disinfection and sterilization procedures of the space industry not only demonstrate their candidacy as extremophiles, but further their candidacy as potential contaminants that may be brought to Mars. The features of these bacteria that allow them to persist in difficult environments on Earth and potentially on Mars should also be considered when checking for contaminants in future missions.

4.3 Molecular biosignatures

Although the presence of colorful pigments in an environment deprived of light, such as lava tubes, could appear surprising, carotenoids and other pigments can play different roles depending on the metabolisms of the host cells. Carotenoid

molecules have a wide distribution in very diverse organisms (more than 750 chemical structures determined to date), including extremophiles, where they serve several key functions at the cellular level. In addition to serving as photoprotective accessory pigments in phototrophic organisms, they have excellent antioxidant properties acting as reactive oxygen species (ROS) scavengers thus protecting cellular DNA and proteins (Stahl & Sies, 2003). They are also believed to help stabilize membranes at low temperatures (Dieser et al., 2018), particularly relevant for Icelandic microbial communities. It has even been proposed that carotenoids played an important role in the early evolution of life on Earth (Alcaíno et al., 2016; Klassen, 2010) by being involved in membrane stabilization, prior to fatty acids (Ourisson & Nakatani, 1994). These functions and properties, essential for the highly UV-irradiated early Earth, might also be compatible with early Mars organisms (Cockell, 2002; Rothschild, 1990), adding to the relevance of carotenoids as a biosignature target for our search for life on Mars. In addition, although we would not normally expect phototrophic organisms in cave environments, cyanobacteria have recently been reported in deep subsurface rock samples on Earth, where they switch to a light-independent hydrogen-based lithoautotrophic metabolism (Puente-Sánchez et al., 2018).

Carotenoids may prove as a critical biosignature in our search for life in extraterrestrial lava tubes as they are only found in living organisms, are relatively easy to distinguish and detect, and have been shown to be highly resistant to oxidative and radiative stress in simulated Martian conditions (Baqué et al., 2016). Portable Raman instruments could potentially detect carotenoid molecules in caves *in situ* by humans or robotic explorers. As lava tubes are shielded from radiation on Mars, carotenoids have the potential to be preserved on even longer timescales. Potential pigmented species found in our DNA analysis of sample C2 occur in the genera *Cupriavidus* and *Methylobacterium.* These are thought to be the source of the carotenoids identified in the sample (Ramachandran et al., 2014; Osawa et al., 2015; Heider et al., 2012). The identification of carotenoids in our samples demonstrate a staying power in this copper-rich environment that may lend itself to future identification in caves as evidence of extant or extinct life.

5 Conclusion

The Planetary Analogues and Exobiology Lava Tube Expedition (PELE) was formed to investigate biosignatures in terrestrial lava tubes and inform the search for extant and extinct life in Martian lava tubes. Our *Study in Blue*, a case study of blue, copper-rich speleothems collected in Icelandic lava tubes, gave insights into how we might approach sampling these analogue environments, and what we might expect to find. A portable XRF gave us a good indication of elemental composition inside the caves and helped us distinguish regions of interest, i.e., secondary minerals with obvious variations in composition to that of the background lava rock. 16S rRNA sequencing of microbial mats revealed Proteobacteria as the dominant bacterial phylum, several carotenoid-containing genera, chemolithoautotrophic genera, and genera known for their high metal

resistance, all characteristics which make them good candidates for surviving on Mars, but also potential contaminants in Mars missions. Raman analysis produced a prominent carotenoid signal, which is a promising biosignature feasibly detectable for robotic lava tube explorers carrying Raman instruments. The morphology and elemental composition of the blue secondary mineral precipitates were elucidated by SEM/EDS, identifying chrysocolla crusts, and a complex, layered precipitate consisting of chrysocolla, pseudomalachite, manganese (hydr)oxide, and a carbonate-bearing species. It appears that copper may be leached from hyaloclastite and ash deposits, enriching the rainwater and groundwater that filters into the caves. Copper-rich speleothems are then precipitated out and serve as biotopes for metal-resistant organisms. As chrysocolla and other oxidized copper mineral phases have been detected on the surface of Mars, they may also be present in Martian lava tubes, and if so, would be worthy targets for astrobiological investigations by future missions.

Acknowledgments

The Icelandic Speleological Society (ISS) was indispensable to this work, with in-depth knowledge of the terrain, and by doing their best to keep these caves in their pristine states by protecting them from human contamination by tourists or civilians, which is vital when collecting samples of microbial mats. Our guides Árni B. Stefánsson, Guðni Gunnarsson, and Ingólfur Páll Matthíasson were delightful to work with, and we thank them with the utmost reverence for their professionalism and for sharing these subterranean natural wonders with our team.

Many thanks to Anett Blischke of the Icelandic GeoSurvey for constructing the geological map of Iceland in Figure 1.

This work was supported by NWO ALWOP.274 and the University of Akureyri Research Fund (grant no. R1812).

M.B. acknowledges the support of the Deutsche Forschungsgemeinschaft (DFG – German Research Foundation) for the project "Raman Biosignatures for Astrobiology Research" (RaBioFAM; project number: 426601242) and of Geo.X, the Research Network for Geosciences in Berlin and Potsdam, for a travel grant.

B.R.S. is an inventor of patents and patent applications involving small molecule therapeutics, co-founded and serves as a consultant to Inzen Therapeutics and Nevrox Limited, and serves as a consultant to Weatherwax Biotechnologies Corporation and Akin Gump Strauss Hauer & Feld LLP.

Open Research

The data supplement to this work is accessible at https://public.yoda.uu.nl/geo/UU01/I32Z95.html, DOI: 10.24416/UU01-I32Z95. The geological map of Iceland was created using ArcGIS 10.8.1 and data at the Iceland GeoSurvey (Hjartarson & Sæmundsson, 2014), available at (https://en.isor.is/geological-maps-geological-web-map) and (https://arcgisserver.isor.is/). Figures were created with Prism software

available at https://www.graphpad.com/scientific-software/prism/, and Krona (Ondov et al., 2011), available at https://github.com/marbl/Krona/releases. The raw DNA sequences were processed with the R package DADA2 (version 1.18.0) (Callahan, McMurdie, et al., 2016). DNA sequencing data was obtained using the Silva_132 database (Quast et al., 2013), available at https://www.arb-silva.de/, and the RDP naïve Bayesian classifier (Wang et al., 2007).

References

Alcaíno, J., Baeza, M., & Cifuentes, V. (2016). Carotenoid distribution in nature. *Carotenoids in Nature*, 3-33. https://doi.org/10.1007/978-3-319-39126-7_1

Anthony, J. W. (1990). *Handbook of mineralogy: Arsenates, phosphates, vanadates.* (Vol. 4). Mineral Data Pub.

Arnalds, O. (2010). *Dust sources and deposition of aeolian materials in Iceland*. https://skemman.is/handle/1946/19921

Arnalds, O. (2015). The Volcanic Aeolian Environments of Iceland. In *The Soils of Iceland* (pp. 139-152). Springer, Dordrecht. https://doi.org/10.1007/978-94-017-9621-7_11

Arnalds, O., Gisladottir, F. O., & Sigurjonsson, H. (2001). Sandy deserts of Iceland: an overview. *Journal of Arid Environments*, *47*(3), 359–371. https://doi.org/10.1006/JARE.2000.0680

Baqué, M., Verseux, C., Böttger, U., Rabbow, E., de Vera, J. P. P., & Billi, D. (2016). Preservation of biomarkers from cyanobacteria mixed with Marslike regolith under simulated Martian atmosphere and UV flux. *Origins of Life and Evolution of Biospheres*, *46*(2–3), 289–310. https://doi.org/10.1007/s11084-015-9467-9

Baqué, M., Hanke, F., Böttger, U., Leya, T., Moeller, R., and Vera, J.-P. de (2018). Protection of cyanobacterial carotenoids' Raman signatures by Martian mineral analogues after high-dose gamma irradiation. *Journal of Raman Spectroscopy. 49*(10), 1617–1627. https://doi.org/10.1002/jrs.5449.

Berger, J. A., Schmidt, M. E., Gellert, R., Boyd, N. I., Desouza, E. D., Flemming, R. L., Izawa, M. R. M., Ming, D. W., Perrett, G. M., Rampe, E. B., Thompson, L. M., VanBommel, S. J. V., & Yen, A. S. (2017). Zinc and germanium in the sedimentary rocks of Gale Crater on Mars indicate hydrothermal enrichment followed by diagenetic fractionation. *Journal of Geophysical Research: Planets*, *122*(8), 1747–1772. https://doi.org/10.1002/2017JE005290

Blank, J. G., Agha-mohammadi, A. A., Bell Jr, E. R., Crown, D. A., Morrell, B., Patterson, C. J., ... & Whelley, P. L. (2021). Volcanic caves as priority sites for astrobiology science. *Bulletin of the American Astronomical Society*, *53*(4), 306. https://doi.org/10.3847/25c2cfeb.1bc1e6cf

Boston, P. J., Spilde, M. N., Northup, D. E., Melim, L. A., Soroka, D. S., Kleina, L. G., Lavoie, K. H., Hose, L. D., Mallory, L. M., Dahm, C. N., Crossey, L. J., & Schelble, R. T. (2001). Cave biosignature suites: microbes, minerals, and mars. *Astrobiology*, *1*(1), 25–55. https://doi.org/10.1089/153110701750137413

Callahan, B. J., Mcmurdie, P. J., Rosen, M. J., Han, A. W., Johnson, A. J. A., & Holmes, S. P. (2016). DADA2: high-resolution sample inference from Illumina amplicon data. *Nature Methods*, *13*(7), 581-583. https://doi.org/10.1038/nMeth.3869

Callahan, B. J., McMurdie, P. J., Rosen, M. J., Han, A. W., Johnson, A. J. A., & Holmes, S. P. (2016). DADA2: High-resolution sample inference from Illumina amplicon data. *Nature Methods*, *13*(7). https://doi.org/10.1038/nmeth.3869

Candela, P. A., & Holland, H. D. (1984). The partitioning of copper and molybdenum between silicate melts and aqueous fluids. *Geochimica et Cosmochimica Acta*, *48*(2), 373–380. https://doi.org/10.1016/0016-7037(84)90257-6

Cockell, C. S. (2002). The Ultraviolet Radiation Environment of Earth and Mars: Past and Present. In G. Horneck & C. Baumstark-Khan (Eds.), *Astrobiology*. Springer Berlin Heidelberg. https://doi.org/10.1007/978-3-642-59381-9_15

Dickinson, W. H., Caccavo, F., & Lewandowski, Z. (1996). The ennoblement of stainless steel by manganic oxide biofouling. *Corrosion Science*, *38*(8), 1407–1422. https://doi.org/10.1016/0010-938X(96)00031-5

Diels, L., van Roy, S., Taghavi, S., & van Houdt, R. (2009). From industrial sites to environmental applications with *Cupriavidus metallidurans*. *Antonie Van Leeuwenhoek*, *96*(2), 247–258. https://doi.org/10.1007/s10482-009-9361-4

Dieser, M., Greenwood, M., Foreman, C. M., & Greenwood, M. (2018). Carotenoid pigmentation in antarctic heterotrophic bacteria as a strategy to withstand environmental stresses. *Arctic, Antarctic, and Alpine Research*, *42*(4), 396–405. https://doi.org/10.1657/1938-4246-42.4.396

Eason, D. E., & Sinton, J. M. (2009). Lava shields and fissure eruptions of the Western Volcanic Zone, Iceland: Evidence for magma chambers and crustal interaction. *Journal of Volcanology and Geothermal Research*, *186*(3–4), 331–348. https://doi.org/10.1016/J.JVOLGEORES.2009.06.009

Furnes, H. (1978). Element mobility during palagonitization of a subglacial hyaloclastite in Iceland. *Chemical Geology*, *22*(C), 249–264. https://doi.org/10.1016/0009-2541(78)90034-7

Giachino, A., & Waldron, K. J. (2020). Copper tolerance in bacteria requires the activation of multiple accessory pathways. *Molecular Microbiology*, *114*(3), 377–390. https://doi.org/10.1111/MMI.14522

Gibson, I. L., Kirkpatrick, R. J., Emmerman, R., Schmincke, H. U., Pritchard, G., Oakley, P. J., Thorpe, R. S., & Marriner, G. F. (1982). The trace element

composition of the lavas and dikes from a 3-km vertical section through the lava pile of eastern Iceland. *Journal of Geophysical Research*, *87*(B8), 6532–6546. https://doi.org/10.1029/JB087IB08P06532

Gounot, A. M. (1994). Microbial oxidation and reduction of manganese: Consequences in groundwater and applications. *FEMS Microbiology Reviews*, *14*(4), 339–349. https://doi.org/10.1111/j.1574-6976.1994.tb00108.x

Gunnarsdottir, M. J., Gardarsson, S. M., st. Jonsson, G., Armannsson, H., & Bartram, J. (2015). Natural background levels for chemicals in Icelandic aquifers. *Hydrology Research*, *46*(4), 647–660. https://doi.org/10.2166/nh.2014.123

Hannesdóttir, H., Zöhrer, A., Davids, H., Sigurgeirsdóttir, S. I., Skírnisdóttir, H., & Árnason, Þ. (2010). Vatnajökull National Park: Geology and Geodynamics. *Northern Environmental Education Development. University of Iceland. Hornafjordur, Iceland: Hornafjordur Regional Research Centre*.

Haraldsson, K. Ö. (2001). *The Hekla 2000 eruption, distribution of ash from the first days of the eruption* (Doctoral dissertation, BSc Thesis, University of Iceland).

Hathaway, J. J. M., Garcia, M. G., Balasch, M. M., Spilde, M. N., Stone, F. D., Dapkevicius, M. D. L. N. E., Amorim, I. R., Gabriel, R., Borges, P. A. V., & Northup, D. E. (2014). Comparison of Bacterial Diversity in Azorean and Hawai'ian Lava Cave Microbial Mats. *Geomicrobiology Journal*, *31*(3), 205–220. https://doi.org/10.1080/01490451.2013.777491

Heider, S. A., Peters-Wendisch, P., & Wendisch, V. F. (2012). Carotenoid biosynthesis and overproduction in *Corynebacterium glutamicum*. *BMC microbiology*, 12(1), 1-11.

Hjartarson, A., & Sæmundsson, K. (2014). Geological map of Iceland, bedrock. 1: 600,000. *Iceland GeoSurvey, Reykjavík*.

Hoffmann, L. J., Breitbarth, E., Ardelan, M. v., Duggen, S., Olgun, N., Hassellöv, M., & Wängberg, S. Å. (2012). Influence of trace metal release from volcanic ash on growth of *Thalassiosira pseudonana* and *Emiliania huxleyi*. *Marine Chemistry*, *132–133*, 28–33. https://doi.org/10.1016/J.MARCHEM.2012.02.003

Huang, H., Zhao, Y., Xu, Z., Ding, Y., Zhang, W., & Wu, L. (2018). Biosorption characteristics of a highly Mn(II)-resistant Ralstonia pickettii strain isolated from Mn ore. *PLOS ONE*, *13*(8), e0203285. https://doi.org/10.1371/JOURNAL.PONE.0203285

Janssen, P. J., van Houdt, R., Moors, H., Monsieurs, P., Morin, N., Michaux, A., Benotmane, M. A., Leys, N., Vallaeys, T., Lapidus, A., Monchy, S., Médigue, C., Taghavi, S., McCorkle, S., Dunn, J., van der Lelie, D., & Mergeay, M. (2010). The complete genome sequence of *Cupriavidus metallidurans* Strain CH34, a master survivalist in harsh and anthropogenic environments. *PLOS ONE*, *5*(5), e10433. https://doi.org/10.1371/JOURNAL.PONE.0010433

Jones, M. T., & Gislason, S. R. (2008). Rapid releases of metal salts

and nutrients following the deposition of volcanic ash into aqueous environments. *Geochimica et Cosmochimica Acta*, *72*(15), 3661–3680. https://doi.org/10.1016/J.GCA.2008.05.030

Kenney, G. E., & Rosenzweig, A. C. (2018). Chalkophores. *Annual Review of Biochemistry*, *87*, 645–676. https://doi.org/10.1146/ANNUREV-BIOCHEM-062917-012300

Kiernan, K., Wood, A. C., & Middleton, A. G. (2003). Aquifer structure and contamination risk in lava flows: insights from Iceland and Australia. *Environmental Geology*, *43*, 852–865. https://doi.org/10.1007/s00254-002-0707-8

Klassen, J. L. (2010). Phylogenetic and evolutionary patterns in microbial carotenoid biosynthesis are revealed by comparative genomics. *PLoS ONE*, *5*(6). https://doi.org/10.1371/journal.pone.0011257

Ladomersky, E., & Petris, M. J. (2015). Copper tolerance and virulence in bacteria. *Metallomics*, *7*(6), 957–964. https://doi.org/10.1039/C4MT00327F

Léveillé, R. J., & Datta, S. (2010). Lava tubes and basaltic caves as astrobiological targets on Earth and Mars: A review. *Planetary and Space Science*, *58*(4), 592–598. https://doi.org/10.1016/j.pss.2009.06.004

Little, B. J., & Wagner, P. A. (2018). Chapter 4. Spatial Relationships Between Bacteria and Mineral Surfaces. In J. F. N. K. H. Banfield (Ed.), *Geomicrobiology: Interactions between Microbes and Minerals* (pp. 123–160). De Gruyter. https://doi.org/10.1515/9781501509247-006

Mason, E., Wieser, P. E., Liu, E. J., Edmonds, M., Ilyinskaya, E., Whitty, R. C. W., Mather, T. A., Elias, T., Nadeau, P. A., Wilkes, T. C., McGonigle, A. J. S., Pering, T. D., Mims, F. M., Kern, C., Schneider, D. J., & Oppenheimer, C. (2021). Volatile metal emissions from volcanic degassing and lava–seawater interactions at Kīlauea Volcano, Hawai'i. *Communications Earth & Environment*, *2*(1). https://doi.org/10.1038/s43247-021-00145-3

McMurdie, P. J., & Holmes, S. (2013). phyloseq: An R Package for Reproducible Interactive Analysis and Graphics of Microbiome Census Data. *PLOS ONE*, *8*(4), e61217. https://doi.org/10.1371/JOURNAL.PONE.0061217

Mergeay, M., van Houdt, R., Hobman, J., Monsieurs, P., & Vandenbussche, G. (2015). *Metal Response in Cupriavidus metallidurans Volume I: From Habitats to Genes and Proteins* (M. Mergeay & R. van Houdt, Eds.). Springer. https://doi.org/10.1007/978-3-319-20594-6

Mijnendonckx, K., Provoost, A., Ott, C. M., Venkateswaran, K., Mahillon, J., Leys, N., & van Houdt, R. (2013). characterization of the survival ability of *Cupriavidus metallidurans* and *Ralstonia pickettii* from space-related environments. *Microbial Ecology*, *65*(2), 347–360. https://doi.org/10.1007/s00248-012-0139-2

Monchy, S., Benotmane, M. A., Janssen, P., Vallaeys, T., Taghavi, S., Van Der

Lelie, D., & Mergeay, M. (2007). Plasmids pMOL28 and pMOL30 of *Cupriavidus metallidurans* are specialized in the maximal viable response to heavy metals. *Journal of bacteriology*, *189*(20), 7417-7425.

Morosov, X., Davoudi, C. F., Baumgart, M., Brocker, M., & Bott, M. (2018). The copper-deprivation stimulon of *Corynebacterium glutamicum* comprises proteins for biogenesis of the actinobacterial cytochrome bc1-aa3 supercomplex. *Journal of Biological Chemistry*, *293*(40), 15628–15640. https://doi.org/10.1074/jbc.RA118.004117

Nealson, K. H., Tebo, B. M., & Rosson, R. A. (1988). Occurrence and Mechanisms of Microbial Oxidation of Manganese. *Advances in Applied Microbiology*, *33*(C), 279–318. https://doi.org/10.1016/S0065-2164(08)70209-0

Northup, D. E., & Lavoie, K. H. (2001). Geomicrobiology of caves: A review. *Geomicrobiology Journal*, *18*(3), 199–222. https://doi.org/10.1080/01490450152467750

Northup, D. E., Melim, L. A., Spilde, M. N., Hathaway, J. J. M., Garcia, M. G., Moya, M., Stone, F. D., Boston, P. J., Dapkevicius, M. L. N. E., & Riquelme, C. (2011). Lava cave microbial communities within mats and secondary mineral deposits: implications for life detection on other planets. *Astrobiology*, *11*(7), 601–618. https://doi.org/10.1089/ast.2010.0562

Northup, D. E., Stefánsson, Á. B., Medina, M. J., Caimi, N. A., & Kooser, A. S. (2016). Microbial communities of Icelandic lava caves. In *Proc 16th Int Symp Vulcanospeleo*, *Ocean View, HI.*

Ondov, B. D., Bergman, N. H., & Phillippy, A. M. (2011). Interactive metagenomic visualization in a Web browser. *BMC Bioinformatics*, *12*. https://doi.org/10.1186/1471-2105-12-385

Osawa, A., Kaseya, Y., Koue, N., Schrader, J., Knief, C., Vorholt, J. A., ... & Shindo, K. (2015). 4-[2-O-11Z-Octadecenoyl- -glucopyranosyl]-4, 4 -diapolycopene-4, 4 -dioic acid and 4-[2-O-9Z-hexadecenoyl- -glucopyranosyl]-4, 4 -diapolycopene-4, 4 -dioic acid: new C30-carotenoids produced by *Methylobacterium*. Tetrahedron Letters, 56(21), 2791-2794.

Ourisson, G., & Nakatani, Y. (1994). The terpenoid theory of the origin of cellular life: the evolution of terpenoids to cholesterol. *Chemistry & Biology*, *1*(1), 11–23. https://doi.org/10.1016/1074-5521(94)90036-1

Payré, V., Fabre, C., Sautter, V., Cousin, A., Mangold, N., Deit, L. le, Forni, O., Goetz, W., Wiens, R. C., Gasnault, O., Meslin, P. Y., Lasue, J., Rapin, W., Clark, B., Nachon, M., Lanza, N. L., & Maurice, S. (2019). Copper enrichments in the Kimberley formation in Gale crater, Mars: Evidence for a Cu deposit at the source. *Icarus*, *321*, 736–751. https://doi.org/10.1016/j.icarus.2018.12.015

Popa, C., Carrozzo, F. G., Achille, D. G., Silvestro, S., Esposito, F., & Mennella, V. (2014). Evidences for copper bearing minerals in Shalbatana Valley, Mars. *45th Lunar and Planetary Science Conference*, 2340.

Puente-Sánchez, F., Arce-Rodríguez, A., Oggerin, M., García-Villadangos, M., Moreno-Paz, M., Blanco, Y., Rodríguez, N., Bird, L., Lincoln, S. A., Tornos, F., Prieto-Ballesteros, O., Freeman, K. H., Pieper, D. H., Timmis, K. N., Amils, R., & Parro, V. (2018). Viable cyanobacteria in the deep continental subsurface. *Proceedings of the National Academy of Sciences*, *115*(42), 10702–10707. https://doi.org/10.1073/PNAS.1808176115

Quast, C., Pruesse, E., Yilmaz, P., Gerken, J., Schweer, T., Yarza, P., Peplies, J., & Glöckner, F. O. (2013). The SILVA ribosomal RNA gene database project: improved data processing and web-based tools. *Nucleic Acids Research*, *41*(D1), D590–D596. https://doi.org/10.1093/NAR/GKS1219

Ramachandran, H., Iqbal, M. A., & Amirul, A. A. (2014). Identification and characterization of the yellow pigment synthesized by *Cupriavidus sp.* USMAHM13. *Applied biochemistry and biotechnology*, 174(2), 461-470.

Rose, W. I., Gu, Y., Watson, I. M., Yu, T., Bluth, G. J. S., Prata, A. J., Krueger, A. J., Krotkov, N. A., Carn, S., Fromm, M. D., Hunton, D. E., Ernst, G. G. J., Viggiano, A. A., Miller, T. M., Ballenthin, J. O., Reeves, J. M., Wilson, J. C., Anderson, B. E., & Flittner, E. (2003). The February-March 2000 eruption of Hekla, Iceland from a satellite perspective. *Geophysical Monograph Series*, *139*, 107–132. https://doi.org/10.1029/139GM07

Rothschild, L. J. (1990). Earth analogs for Martian life. Microbes in evaporites, a new model system for life on Mars. *Icarus*, *88*(1), 246–260. https://doi.org/10.1016/0019-1035(90)90188-F

Rudnick, R. L., & Gao, S. (2003). Composition of the continental crust. *Treatise on Geochemistry*, *3–9*, 1–64. https://doi.org/10.1016/B0-08-043751-6/03016-4

Sanyal, S. K., Reith, F., & Shuster, J. (2020). A genomic perspective of metal-resistant bacteria from gold particles: Possible survival mechanisms during gold biogeochemical cycling. *FEMS Microbiology Ecology*, *96*(7), fiaa111.

Sato, Y., Nishihara, H., Yoshida, M., Watanabe, M., Rondal, J. D., Concepcion, R. N., & Ohta, H. (2006). *Cupriavidus pinatubonensis sp. nov.* and *Cupriavidus laharis sp. nov.*, novel hydrogen-oxidizing, facultatively chemolithotrophic bacteria isolated from volcanic mudflow deposits from Mt. Pinatubo in the Philippines. *International Journal of Systematic and Evolutionary Microbiology*, *56*, 973–978. https://doi.org/10.1099/ijs.0.63922-0

Sauro, F., Pozzobon, R., Massironi, M., de Berardinis, P., Santagata, T., & de Waele, J. (2020). Lava tubes on Earth, Moon and Mars: A review on their size and morphology revealed by comparative planetology. In *Earth-Science Reviews* (Vol. 209). Elsevier B.V. https://doi.org/10.1016/j.earscirev.2020.103288

Schmincke, H. U., Viereck, L. G., Griffin, B. J., & Pritchard, R. G. (1982). Volcaniclastic rocks of the Reydarfjördur drill hole, eastern Iceland: 1. Primary features. *Journal of Geophysical Research: Solid Earth*, *87*(B8), 6437-6458. https//doi.org/10.1029/JB087iB08p06437

Schock, M. R., Lytle, D. A., & Clement, J. A. (1995). Effect of pH, DIC, orthophosphate and sulfate on drinking water cuprosolvency. In *National Risk Management Research Lab Technical Report*. https://www.osti.gov/biblio/128476

Schulze-Makuch, D., & Irwin, L. N. (2004). *Life in the Universe*. Springer-Verlag.

Selensky, M. J., Masterson, A. L., Blank, J. G., Lee, S. C., & Osburn, M. R. (2021). Stable carbon isotope depletions in lipid biomarkers suggest subsurface carbon fixation in lava caves. *Journal of Geophysical Research: Biogeosciences*, *126*(7). https://doi.org/10.1029/2021JG006430

Sheth, H. (2018). Explosive Volcanism in Flood Basalt Provinces. *A Photographic Atlas of Flood Basalt Volcanism*, 171–194. https://doi.org/10.1007/978-3-319-67705-7_7

Smith, D. B., Zielinski, R. A., & Rose, W. I. (1982). Leachability of uranium and other elements from freshly erupted volcanic ash. *Journal of Volcanology and Geothermal Research*, *13*(1–2), 1–30. https://doi.org/10.1016/0377-0273(82)90017-8

Stahl, W., & Sies, H. (2003). Antioxidant activity of carotenoids. *Molecular Aspects of Medicine*, *24*(6), 345–351. https://doi.org/10.1016/S0098-2997(03)00030-X

Stivaletta, N., Barbieri, R., & Billi, D. (2012). Microbial colonization of the salt deposits in the driest place of the Atacama Desert (Chile). *Origins of Life and Evolution of Biospheres*, *42*(2), 187–200. https://doi.org/10.1007/s11084-012-9289-y

Thordarson, T., & Self, S. (1993). The Laki (Skaftár Fires) and Grímsvötn eruptions in 1783–1785. *Bulletin of Volcanology*, *55*(4), 233-263.

Uckert, K., Chanover, N. J., Getty, S., Voelz, D. G., Brinckerhoff, W. B., Mcmillan, N., Xiao, X., Boston, P. J., Li, X., Mcadam, A., Glenar, D. A., & Chavez, A. (2017). The characterization of biosignatures in caves using an instrument suite. *Astrobiology*, *17*(12), 1203–1218. https://doi.org/10.1089/ast.2016.1568

Vítek, P., Osterrothová, K., & Jehlička, J. (2009). Beta-carotene—a possible biomarker in the Martian evaporitic environment: Raman micro-spectroscopic study. *Planetary and Space Science*, *57*(4), 454-459. https//doi.org/10.1016/j.pss.2008.06.001

von Rozycki, T., & Nies, D. H. (2009). Cupriavidus metallidurans: evolution of a metal-resistant bacterium. *Antonie van Leeuwenhoek*, *96*(2), 115–139. https://doi.org/10.1007/S10482-008-9284-5

Wang, Q., Garrity, G. M., Tiedje, J. M., & Cole, J. R. (2007). Naïve Bayesian classifier for rapid assignment of rRNA sequences into the new bacterial taxonomy. *Applied and Environmental Microbiology*, *73*(16), 5261–5267. https://doi.org/10.1128/AEM.00062-07/

Yang, E., Sun, · Leni, Ding, · Xiaoyuan, Dongdong Sun, ·, Liu, J., & Wang, W. (2019). Complete genome sequence of *Caulobacter flavus* RHGG3 T, a type species of the genus Caulobacter with plant growth-promoting traits and heavy metal resistance. *3 Biotech*, *9*(2), 42. https://doi.org/10.1007/s13205-019-1569-z

Earth and Space Science

Supporting Information for

A Study in Blue: Secondary Copper-rich Minerals and their Associated Bacterial Diversity in Icelandic Lava Tubes

Nina Kopacz[1], Joleen Csuka[2], Mickael Baqué[3], Iaroslav Iakubivskyi[4], Hrefna Guðlaugardóttir[5], Ingeborg J. Klarenberg[5,6], Mahid Ahmed[1], Alexandra Zetterlind[1], Abhijeet Singh[7], Inge Loes ten Kate[1], Eric Hellebrand[1], Brent R. Stockwell[2,8], Árni B. Stefánsson[9], Oddur Vilhelmsson[5,6,10], Anna Neubeck[7], Anna Schnürer[11], Wolf Geppert[12]

[1]Department of Earth Science, Utrecht University, the Netherlands, [2]Department of Chemistry, Columbia University, USA, [3]Institute of Planetary Research, German Aerospace Centre (DLR), Germany, [4]Tartu Observatory, University of Tartu, Estonia, [5]University of Akureyri, Iceland, [6]University of Iceland Biomedical Center, Iceland, [7]Department of Earth Sciences, Uppsala University, [8]Department of Biological Sciences, Columbia University, USA, [9]Augnlæknastofa ÁBS, Iceland, [10]University of Reading School of Biological Sciences, UK, [11]Swedish University of Agricultural Sciences, Sweden, [12]Stockholm University Astrobiology Centre, Sweden.

Contents of this file

Introduction

Additional EDS spectra of the geological thin sections analyzed with SEM/EDS are shown here. Figure S1 shows additional EDS spectra of the thin section in Figure 7 of the manuscript. Figure S2 shows additional spectra of the thin section in Figure 9 of the manuscript.

EDS spectra were obtained with a windowless Oxford Instruments Ultim-Extreme EDS detector. Point ID measurements (30 s counting time) were acquired at voltage of 20 keV and 1 nA, using Oxford Instruments Aztec software v5.1. For improved spatial chemical resolution in finely zoned domains, an accelerating voltage of 10 keV was used, acquiring the L-alpha intensity of Cu.

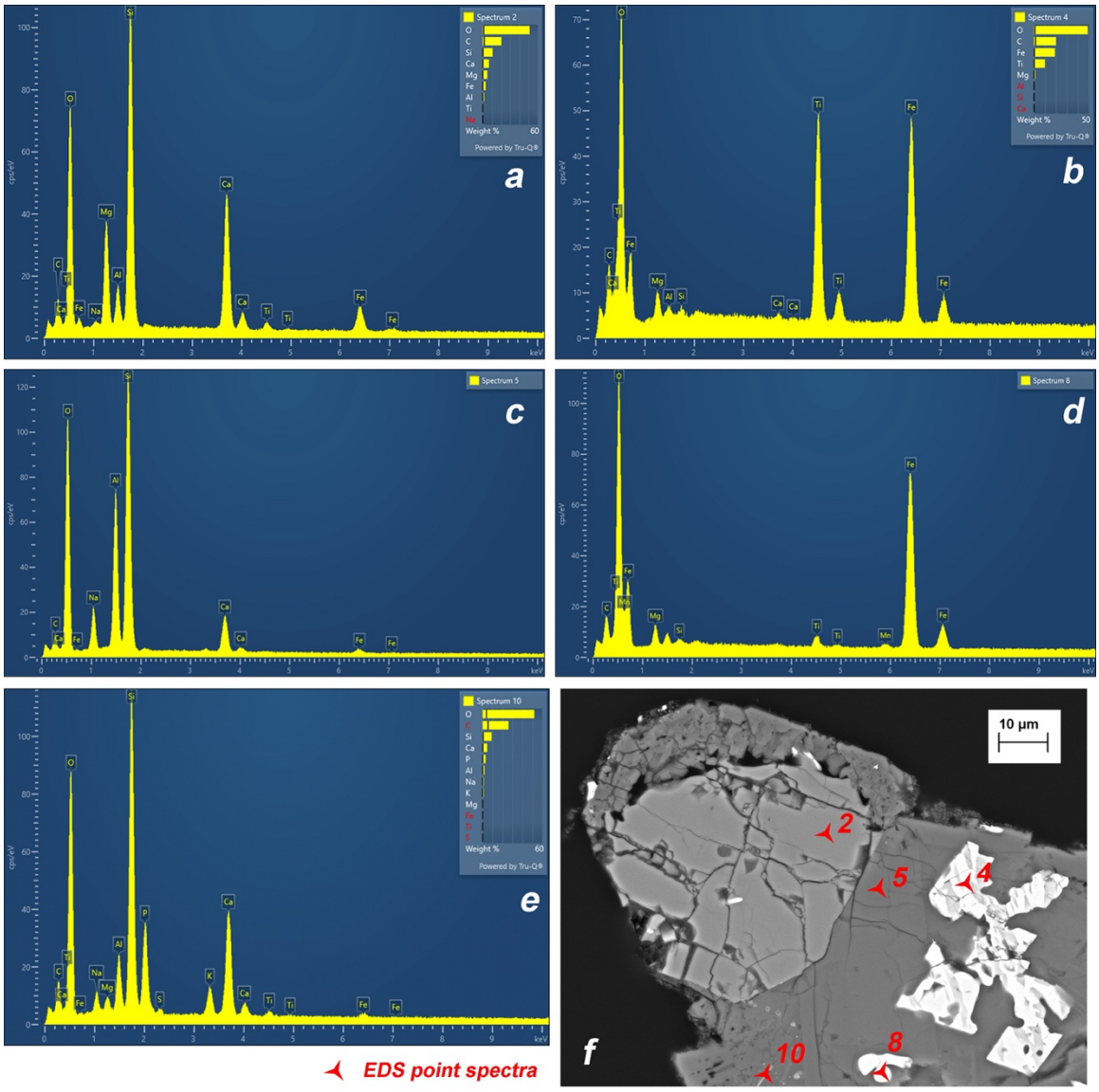

Figure S1. Igneous mineralogy. **(f)** Backscattered electron (BSE) image of sample H7 thin section. **(a-e)** EDS point spectra taken of marked spots in **(f)**, revealing typical basaltic mineralogy: augitic clinopyroxene **(a)**, dendritic titano-magnetite, (oxy-) exsolved into a fine intergrowth of Ti-poor magnetite (white) and ilmenite (slightly less bright) **(b)**, plagioclase **(c)**, magnetite **(d)**, and apatite growth, indicating a highly evolved interstitial melt pocket **(e)**.

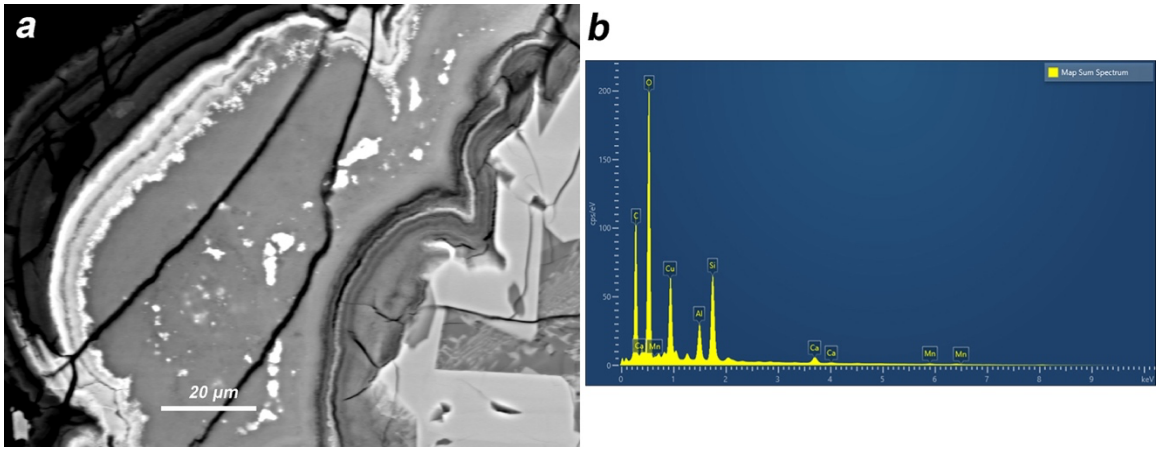

Figure S2. Complex secondary mineral precipitate. **(a)** BSE image of a secondary mineral crust deposited on the edge of the igneous rock in sample B5 thin section. **(b)** EDS sum spectrum of **(a)** showing carbon, copper, and manganese enrichment.